

ARTICLE

# The immunodominant antibody response to Zika virus NS1 protein is characterized by cross-reactivity to self

Cecilia B. Cavazzoni<sup>1,2</sup>, Vicente B.T. Bozza<sup>1</sup>, Tostes C.V. Lucas<sup>1</sup>, Luciana Conde<sup>1</sup>, Bruno Maia<sup>3</sup>, Luka Mesin<sup>2</sup>, Ariën Schiepers<sup>2</sup>, Jonatan Ersching<sup>2</sup>, Romulo L.S. Neris<sup>3</sup>, Jonas N. Conde<sup>4</sup>, Diego R. Coelho<sup>4</sup>, Tulio M. Lima<sup>5</sup>, Renata G.F. Alvim<sup>5</sup>, Leda R. Castilho<sup>5</sup>, Heitor A. de Paula Neto<sup>6</sup>, Ronaldo Mohana-Borges<sup>4</sup>, Irania Assunção-Miranda<sup>3</sup>, Alberto Nobrega<sup>3</sup>, Gabriel D. Victora<sup>2</sup>, and Andre M. Vale<sup>1</sup>

**Besides antigen-specific responses to viral antigens, humoral immune response in virus infection can generate polyreactive and autoreactive antibodies. Dengue and Zika virus infections have been linked to antibody-mediated autoimmune disorders, including Guillain-Barré syndrome. A unique feature of flaviviruses is the secretion of nonstructural protein 1 (NS1) by infected cells. NS1 is highly immunogenic, and antibodies targeting NS1 can have both protective and pathogenic roles. In the present study, we investigated the humoral immune response to Zika virus NS1 and found NS1 to be an immunodominant viral antigen associated with the presence of autoreactive antibodies. Through single B cell cultures, we coupled binding assays and BCR sequencing, confirming the immunodominance of NS1. We demonstrate the presence of self-reactive clones in germinal centers after both infection and immunization, some of which present cross-reactivity with NS1. Sequence analysis of anti-NS1 B cell clones showed sequence features associated with pathogenic autoreactive antibodies. Our findings demonstrate NS1 immunodominance at the cellular level as well as a potential role for NS1 in ZIKV-associated autoimmune manifestations.**

## Introduction

The protective function of antibodies is instrumental for the control of most viral infections. However, in addition to antigen-specific responses to viral antigens, it has long been noted that viral infection can be accompanied by the appearance of polyreactive and often autoreactive antibodies of unknown function (Hunziker et al., 2003). Emergence of self-reactive Igs has been reported for multiple viral diseases; these autoreactive antibodies have the potential to lead to autoimmune manifestations, which can be transient or long-lasting (reviewed in Root-Bernstein and Fairweather, 2014). The origin of the stimulus driving autoantibody generation in viral infection remains controversial. On one hand, antigen mimicry between viral and self-antigens may explain the appearance of selected autoantibodies. Alternatively, a role for cytokine storm leading to nonspecific, polyclonal B cell activation followed by disruption of B cell repertoire homeostasis and self-tolerance has also been proposed (Balakrishnan et al., 2011).

Recently, dengue virus (DENV) and Zika virus (ZIKV) infections have been linked to the occurrence of autoimmune disorders of vascular, ophthalmic, or neurological origin, including Guillain-Barré syndrome (Barbi et al., 2018; de Oliveira et al., 2017), in which autoantibodies seem to play a prominent role (Lardone et al., 2010). A unique feature of DENV, ZIKV, and other flaviviruses is the abundant secretion of the nonstructural protein 1 (NS1) in its hexameric form by infected cells (Akey et al., 2014; Brown et al., 2016; Cox et al., 2015; Young et al., 2000). While intracellular NS1 was shown to be necessary for viral replication, its role as an extracellular soluble factor is poorly understood (Hilgenfeld, 2016). It has recently been shown that NS1 can lead to endothelial dysfunction (Puerta-Guardo et al., 2019; Biering et al., 2021). Moreover, work from multiple groups has shown that NS1 is highly immunogenic (Freire et al., 2017; Gao et al., 2018; Stettler et al., 2016). Notably,

<sup>1</sup>Laboratório de Biologia de Linfócitos, Instituto de Biofísica Carlos Chagas Filho, Universidade Federal do Rio de Janeiro, Rio de Janeiro, Brazil; <sup>2</sup>Laboratory of Lymphocyte Dynamics, The Rockefeller University, New York, NY; <sup>3</sup>Instituto de Microbiologia Paulo de Góes, Universidade Federal do Rio de Janeiro, Rio de Janeiro, Brazil; <sup>4</sup>Laboratório de Genômica Estrutural, Instituto de Biofísica Carlos Chagas Filho, Universidade Federal do Rio de Janeiro, Rio de Janeiro, Brazil; <sup>5</sup>Programa de Engenharia Química, Laboratório de Engenharia de Cultivos Celulares, Instituto Alberto Luiz Coimbra de Pós-Graduação e Pesquisa de Engenharia, Universidade Federal do Rio de Janeiro, Rio de Janeiro, Brazil; <sup>6</sup>Laboratório de Alvos Moleculares, Faculdade de Farmácia, Universidade Federal do Rio de Janeiro, Rio de Janeiro, Brazil.

Correspondence to André M. Vale: [valeam@biof.ufrj.br](mailto:valeam@biof.ufrj.br)

In memory of Dr. Ersching, who died October 2020.

© 2021 Cavazzoni et al. This article is distributed under the terms of an Attribution–Noncommercial–Share Alike–No Mirror Sites license for the first six months after the publication date (see <http://www.rupress.org/terms/>). After six months it is available under a Creative Commons License (Attribution–Noncommercial–Share Alike 4.0 International license, as described at <https://creativecommons.org/licenses/by-nc-sa/4.0/>).

antibodies to DENV NS1 can attenuate the outcome of severe dengue, and vaccination with ZIKV and DENV NS1 have been shown to be protective in animal models (Gonçalves et al., 2015; Richner et al., 2017; Bailey et al., 2019; Beatty et al., 2015). These studies suggest a role for NS1 in the pathogenesis of flavivirus infections, as well as a protective role for anti-NS1 antibodies. However, anti-DENV NS1 antibodies have also been implicated in autoreactivity and may contribute to dengue pathology, possibly through antigen mimicry between NS1 and components of self (Chuang et al., 2016; Lee et al., 2020; Falconar, 1997; Reyes-Sandoval and Ludert, 2019); these observations raise concerns about the safety of NS1 as a vaccine antigen, and further studies are necessary to understand the humoral immune response to this molecule.

Studies of the pathogenesis of human viral infections in animal models face several limitations due to innate viral resistance of mouse species to many human viruses. For this reason, multiple groups have developed models that rely on immunocompromised mice, such as IFNAR-deficient strains, which show greater susceptibility to viral infections (Zellweger et al., 2010; Lazear et al., 2016; Yauch and Shrestha, 2008; Bardina et al., 2017). Although such strategies are useful in studies of viral pathology, they are less useful for the analysis of humoral immune responses, as type I IFNs broadly influence adaptive immunity and directly impact activation of B cells by modulating B cell receptor (BCR) signaling (Demengeot et al., 1997; Kiefer et al., 2012), possibly also affecting clonal selection and entry into germinal centers (GCs; Fallet et al., 2016). For these reasons, an immunocompetent mouse model of ZIKV infection is preferred for the study of antibody response. Accordingly, recent studies have used such models to characterize the T cell (Winkler et al., 2017; Pardy et al., 2017; Huang et al., 2017) and neutralizing antibody response to ZIKV (Dai et al., 2016). Using immunocompetent mouse models, we and others have shown that CD4<sup>+</sup> T cells activate a robust IFN $\gamma$ -dependent B cell response, which is associated with production of neutralizing IgG2a antibodies that bind to ZIKV envelope proteins, including envelope protein domain III (EDIII), and have been associated with virus neutralization. Of note, passive transfer of serum from infected immunocompetent A129 mice protected immunocompromised mice against lethal heterologous challenge with ZIKV (Lucas et al., 2018; Hassert et al., 2018; Elong Ngono et al., 2019).

In the present study, we investigated the humoral immune response to ZIKV NS1 using an immunocompetent mouse model of ZIKV infection as well as NS1 immunization. The antibody response in infected animals showed that NS1 is an immunodominant viral antigen. Importantly, humoral response to NS1 is associated with the presence of autoreactive antibodies, both after infection and immunization. In-depth analysis of B cell clonal selection in GCs, coupling single-B cell cultures with BCR sequencing, confirmed the strong immunodominance of NS1 and revealed the presence of frequent self-reactive clones among GC B cells, some of which cross-reacted with NS1. Anti-NS1 B cell clones were enriched in charged amino acid residues in complementarity determining region 3 of the Ig heavy chain (CDR-H3), a feature shared by self-reactive clones (Wardemann

et al., 2003; Radic and Weigert, 1995). Anti-NS1 clones also showed low levels of somatic hypermutation (SHM) possibly indicative of adaptation of the germline repertoire to this antigen. The presence of self-reactive B cell clones in GCs, formed in response to an immunodominant viral antigen, strongly supports a break of tolerance at the cellular level. Taken together, these findings indicate the potential relevance of NS1 for ZIKV pathogenicity and its associated autoimmune manifestations.

## Results

### Immunocompetent BALB/c mice develop a specific antibody response to ZIKV infection focused on NS1

To study the humoral immune response to ZIKV infection in immunocompetent mice, we injected young adult BALB/c WT mice i.v. with  $10^6$ – $10^7$  PFUs of the Brazilian ZIKV isolate PE243 (Coelho et al., 2017) and followed antibody responses for 50 d postinfection (d.p.i.; Fig. 1 A). Mice showed increased spleen weight from day 7 to 28 after infection (Fig. 1 B), as well as altered total serum Ig concentrations. Increased serum IgM was detected at 7 d.p.i. (Fig. 1 C) and total serum IgG concentration increased progressively between 7 and 21 d.p.i., stabilizing at a higher concentration than controls for up to 50 d.p.i. (Fig. 1 D).

Serum IgM binding to envelope proteins peaked at 7 d.p.i. (Fig. 1 E) followed by a peak in IgG at 14 d.p.i. (Fig. 1 F), as detected using ZIKV-like particles that display proteins E and M in their mature form (Alvim et al., 2019). EDIII is a target of neutralizing antibodies for different flaviviruses (Dai et al., 2016; Beasley and Barrett, 2002; Oliphant et al., 2005; Shrestha et al., 2010). We therefore also assayed serum samples for IgG binding to this portion of the E protein. We found that EDIII-specific IgG peaked in serum at 14 d.p.i. (Fig. 1 G), at which point serum neutralizing activity was also observed (data not shown).

We next searched for NS1-binding IgM and IgG antibodies in sera of infected mice. NS1 is known to be abundantly secreted into the extracellular milieu by flavivirus-infected cells (Watterson et al., 2016) and is highly immunogenic (Brown et al., 2016). IgM binding to NS1 remained almost unchanged compared with uninfected controls (Fig. 1 H). Interestingly, although serum IgG specific to NS1 appeared later than that targeting envelope proteins, anti-NS1 IgG increased progressively after infection, remaining at very high levels for as long as 50 d.p.i. (Fig. 1 I). Since viral RNA was undetectable in blood and brain tissue, in order to investigate whether our observations were dependent on viral replication leading to secretion of NS1 protein by infected cells, we performed the same experiment with UV-inactivated virus. Mice were injected i.v. with  $10^6$ – $10^7$  PFUs of UV-inactivated ZIKV (UV-iZIKV) or replicative ZIKV isolate PE243 (Coelho et al., 2017) and evaluated for 60 d.p.i. (Fig. S1 A). UV-iZIKV did not induce an increase in spleen weight (Fig. S1 B). Despite the presence of E protein-specific IgG in serum (Fig. S1 C), these Ig's did not target domain III (Fig. S1 D), and NS1-specific IgG was not detected (Fig. S1 E). Taken together, these results demonstrate that, although immunocompetent mice survive ZIKV infection with few or no clinical signs, infection with replicative virus induced a robust humoral

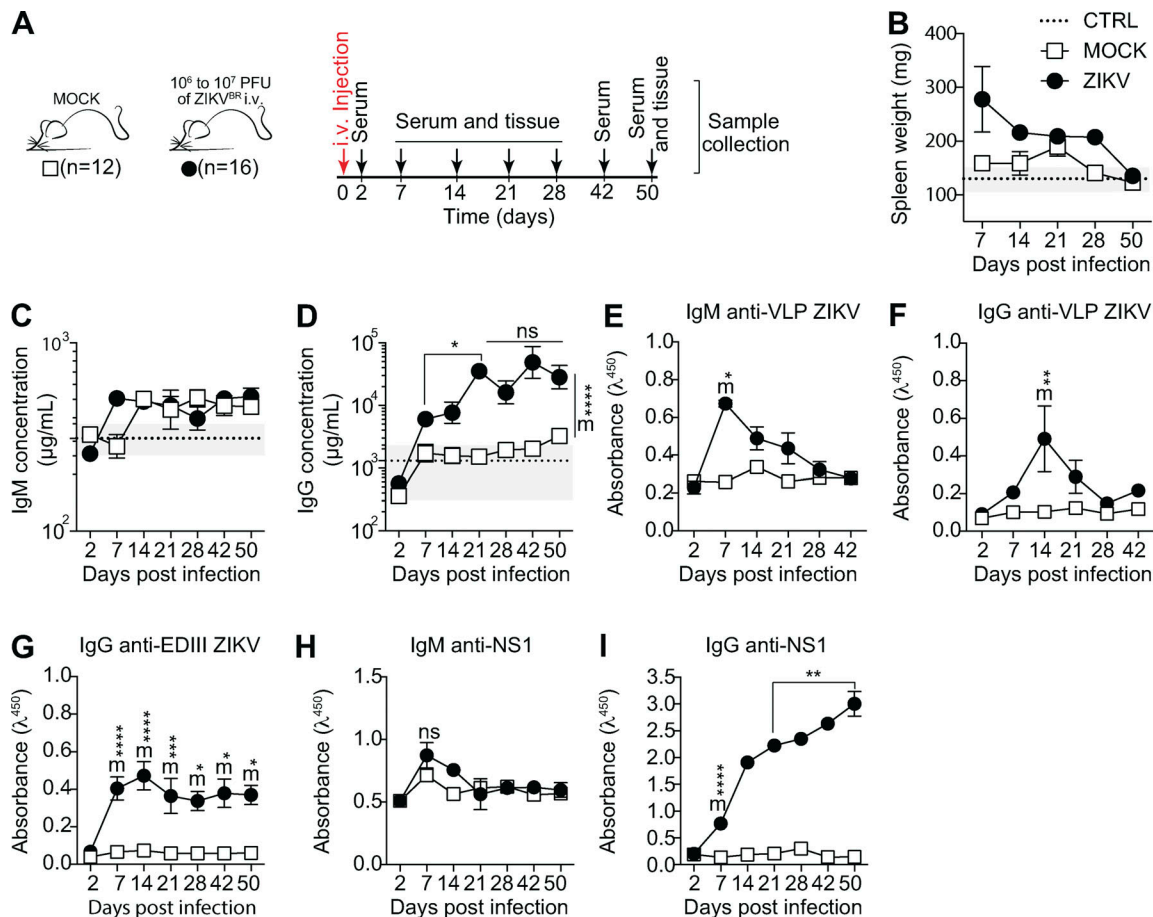


**Figure 1. Characterization of ZIKV infection in immunocompetent BALB/c mice.** (A) Experimental design indicating the time points of serum samples and lymphoid tissue collections. (B) Spleen weight measured at the time of collection, as indicated. (C and D) Total serum IgM (C) and IgG (D) from infected (ZIKV) and control (MOCK) mice, measured by ELISA. (E–G) Levels of IgM and IgG specific for viral surface antigens were measured by ELISA (1:120 dilution) using VLPs and recombinant domain III of ZIKV envelope protein (EDIII). (H and I) Levels of IgM (H) and IgG (I) specific for NS1 protein were measured by ELISA (1:120 dilution) using recombinant ZIKV NS1. Data are representative of three independent experiments with 8–16 mice per group. Statistical analyses were performed using the paired two-tailed Student’s *t* test. \*, *P* ≤ 0.05; \*\*, *P* ≤ 0.01. Mice from different groups were compared using the unpaired two-tailed Student’s *t* test. ZIKV significantly different from MOCK: m\*, *P* ≤ 0.05; m\*\*, *P* ≤ 0.01; m\*\*\*, *P* ≤ 0.001; m\*\*\*\*, *P* ≤ 0.0001. Error bars represent SEM.

immune response, which became progressively dominated by antibodies to the NS1 antigen.

**Dominance of NS1-binding IgG in serum correlates with the emergence of autoreactive antibodies**

The increasing levels of anti-NS1 IgG antibodies from 21 d.p.i. onwards prompted us to further investigate the NS1-specific response in infected mice. Serum titration at different time points suggested an increase in concentration or affinity of IgG for the viral antigen (Fig. 2 A). Endpoint titers increased gradually to ~200,000 at the latest time point assayed (Fig. 2 B). Serum IgG was predominantly of the IgG2a isotype throughout infection, as expected for antiviral responses (Coutelier et al., 1987). Of note, there was a late contribution of IgG1 to total serum IgG titer (Fig. 2, C and D). Given that gamma 1 constant region gene is located upstream of gamma 2a, ruling out sequential switching between these isotypes, our data suggest continued engagement of B cell clones after the initial phase of the response. We also assessed the binding of IgG to closely related DENV antigens. As observed in human antibody response

to ZIKV infection (Stettler et al., 2016; Wang et al., 2017), we found cross-reactivity between ZIKV EDIII and DENV EDIII (Fig. 2 E; and Fig. S2, A and B), whereas ZIKV NS1-specific IgG did not cross-react with DENV NS1 protein (Fig. 2 F; and Fig. S2, C and D).

In addition to the presence of virus-specific antibody responses, viral infections are often associated with hyperglobulinemia due to nonspecific polyclonal activation of B lymphocytes (Hunziker et al., 2003). To assess the potential of ZIKV infection to induce a polyclonal, nonspecific humoral immune response, we looked for IgG binding to unrelated antigens such as heat shock proteins from both mammalian and commensal bacterial origins, which are commonly targeted by autoantibodies in different systems (Fig. S2, E and F; Victora et al., 2007; Füst et al., 2005; Quintana and Cohen, 2011). IgG binding to unrelated antigens, possibly due to polyreactivity, was present at early time points and rapidly decayed, following the kinetics of antibody response to viral structural proteins shown in Fig. 1. Interestingly, serum IgG from ZIKV-infected mice also displayed widespread binding to self-antigens, as revealed using a

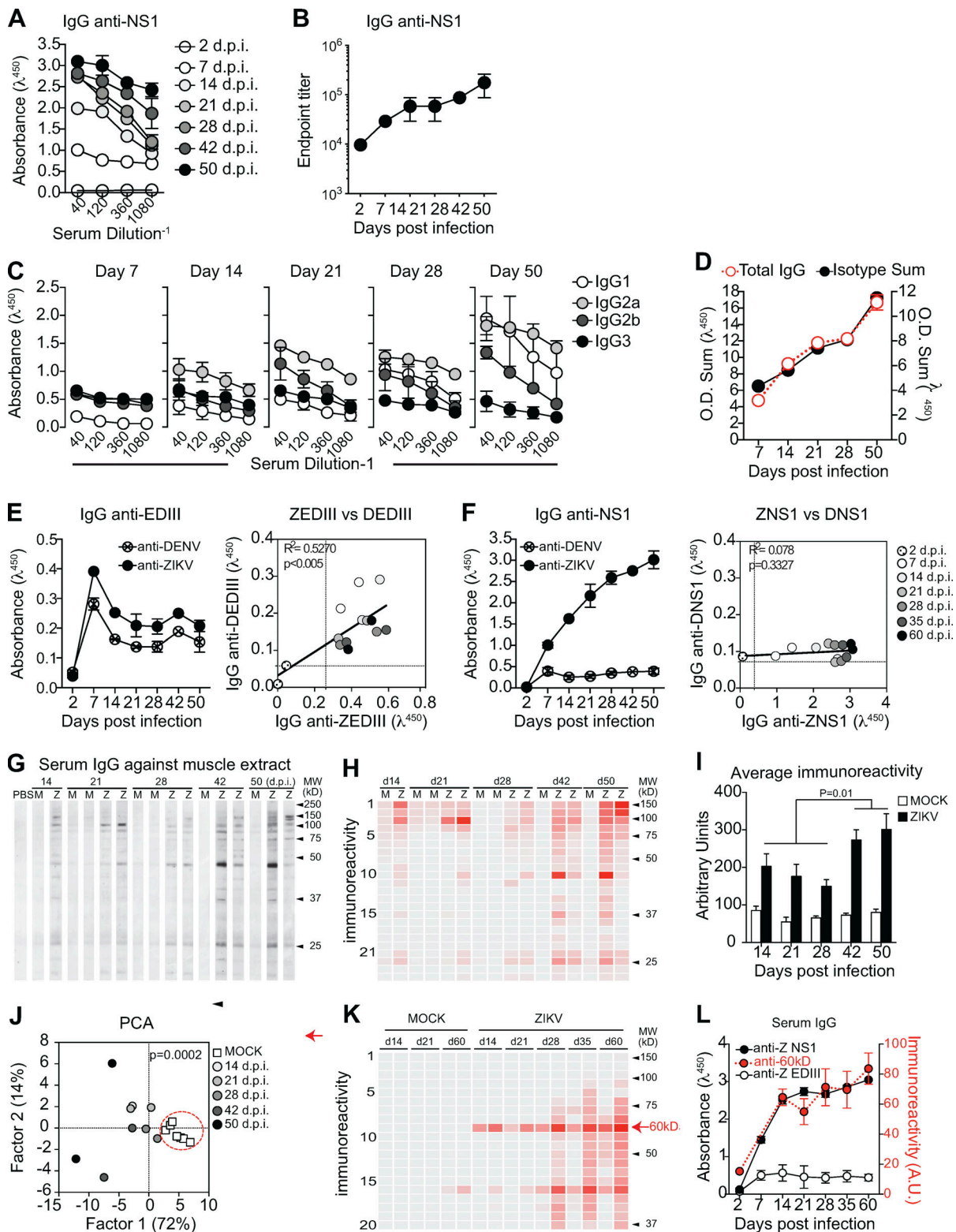


Figure 2. **Humoral immune response to NS1 during ZIKV infection correlates with autoreactive antibodies.** (A) Binding of serum IgG to ZIKV NS1 protein during infection detected by ELISA. (B) Endpoint titer of serum IgG specific to ZIKV NS1 protein after infection. (C) NS1-specific serum IgG isotype composition during experimental infection were detected by antigen-specific ELISA. (D) Total NS1-specific IgG in serum corresponds to the sum of IgG isotypes, present in distinct proportions after infection. O.D., optical density. (E and F) Sera from ZIKV-infected mice (1:120 dilution) were tested by ELISA for binding to ZIKV and DENV antigens EDIII (E) and NS1 (F). Correlation coefficients show cross-reactivity of EDIII-specific IgG, but not of NS1-specific IgG. Correlations were computed as Pearson's correlation coefficients. (G) Self-reactivities present in serum IgG (diluted 1:100) from control (M) and infected (Z) mice using muscle extract from BALB/c mice as source of self-antigens. (H) Intensity of bands was quantified and plotted as a heat map. (I) Total immunoreactivity (sum of all bands intensities) present in the sera of infected (ZIKV) and control (MOCK) mice for each time point after infection. Statistical analyses were performed using

two-tailed Student's *t* test. **(J)** Principal-component analysis (PCA) of all self-reactivities at all time points. Circle indicates the segregation of the control group. Statistical analyses were performed using two-tailed Student's *t* test to compare factor 1 scores of MOCK vs ZIKV. **(K)** Intensity of reactivities present in serum IgG (diluted 1:100) from control (MOCK) and infected mice (ZIKV) using HEP-2 cell extract as source of self-antigens. **(L)** Intensity of the reactivity to a selected 60-kD self-antigen throughout time after infection correlates with levels of serum IgG specific to ZIKV NS1 protein, but not with levels of IgG specific to domain III of ZIKV envelope protein (ZEDIII). A.U., arbitrary units. Data for A and B are from one experiment with three mice per group. Data for C and D are from one experiment representative of two independent experiments with 5–16 mice per group. Data for E, F, K, and L are from one experiment representative of two independent experiments with two to three mice per group. Data for G–J are from one experiment representative of two independent experiments (two representative samples per group are shown). Error bars represent SEM.

semiquantitative immunoblot assay that enables global analysis of the self-reactivity of antibodies present in serum (Nobrega et al., 1993; Haury et al., 1994). Accordingly, at 14 d.p.i., ZIKV-infected mice exhibited serum IgG reactivity to multiple self-antigens from syngeneic brain and muscle tissues (Fig. 2 G), suggesting a break in self-tolerance during the early humoral immune response.

Since polyclonal B cell activation and nonspecific poly-reactive responses are mostly present in the acute phase of the immune response to viral infections and do not contribute meaningfully to serum IgG titers at later time points when infection subsides, we evaluated whether self-antigen reactivity declined at later time points after infection. Strikingly, serum IgG self-reactivity was progressively stronger at later time points (Fig. 2, G–I). Of note, although different mice shared several reactivities toward antigens with similar migration patterns (Fig. 2, G and H), individual immunoreactivity profiles did not necessarily converge in time toward a unique reactivity profile (Fig. 2 J).

To further investigate the progressive increase of self-reactive IgG following infection, we tested serum samples from an additional cohort of ZIKV-infected mice for binding to a HEP-2 cell line extract. These cells are frequently used in standard clinical assays for anti-nuclear antibodies and as a source of cytoplasmic self-antigens (Wardemann et al., 2003). Consistently, a broad range of immunoreactivities arose over time after infection (Fig. 2 K). The levels of IgG reactive to a 60-kD self-antigen paralleled those of NS1-specific, but not EDIII-specific, IgG over time (Fig. 2 L). The overlapping kinetics of anti-NS1 response and self-reactive serum IgG led us to hypothesize there could be a link between the maintenance of autoreactive antibodies and a dominant and sustained anti-NS1 antibody response.

### Virus-specific and autoreactive B cell clones are present in GCs after ZIKV infection

Viral infections typically induce T cell-dependent antibody responses, in which follicular (FO) B cells enter GC reactions where they undergo clonal expansion, SHM, and selection, leading to antibody affinity maturation (reviewed in Victora and Nussenzweig, 2012). After i.v. ZIKV infection, we observed abundant GC formation in spleen. Frequencies of different splenic B cell populations were found to be altered; the reduction in frequency of FO B cells likely reflected GC formation and correlated with levels of serum IgG specific to ZIKV proteins. GC B cell frequency peaked at day 14 after infection and started to decrease by day 21, receding to background levels at 28 d.p.i. (Fig. 3 A).

To investigate the possible link between the antibody response to NS1 and the presence of self-reactive IgG in serum, we devised an experimental strategy that allowed us to more appropriately compare GC B cells between infected and immunized mice. For that purpose, mice were s.c. infected in the footpad with ZIKV, and draining LNs were collected on different days after infection to isolate GC B cells (Fig. 3 B). Consistent with our previous results, we found increasing levels of IgG binding to ZIKV NS1 in serum up to 45 d after s.c. infection. This increase was not observed when the same amount of UV-iZIKV was injected, corroborating the requirement of replicative ZIKV infection for this phenomenon (Fig. 3 C). We could also observe GC formation in LNs after both ZIKV infection and iZIKV immunization, although the latter were both of lower magnitude and shorter in duration (Fig. 3, D and E). At 14 d.p.i., corresponding to the peak of the response, we isolated and cultured GC B cells for Ig production *in vitro*. GC B cell cultures were performed as described by Kuraoka et al. (2016), with modifications, including not adding IL-4 to prevent *in vitro* class switching. As a result, the proportions of IgG isotypes found in culture supernatants broadly matched those of ZIKV-specific antibodies in serum (Fig. S3).

Using limiting dilution analysis, we were able to estimate the frequency of GC B cells secreting Igs binding to virus-like particles (VLPs) or NS1 (Fig. 3, F and G), as well as to self-antigens (Fig. 3 H). Quantification of the number of responding B cell clones per culture ensures accurate determination of the frequency of GC B cells reactive to a given antigen (Nobrega et al., 1998; Vale et al., 2012). GC B cells from mock-, iZIKV-, and ZIKV-injected mice showed similar frequencies of response to polyclonal LPS stimulus, with 30–50% of GC B cells proliferating and differentiating into IgG-secreting plasma cells in all conditions (Fig. S3 A and data not shown). At 14 d.p.i., no reactivity to viral surface antigens was detected in GC B cells derived from control mice (mock) and less than 0.1% of GC B cells from iZIKV-immunized mice secreted IgG that bound detectably to VLPs. Moreover, we were unable to detect GC B cell clones secreting NS1-reactive IgG in either mock- or iZIKV-immunized mice (data not shown). On the other hand, in ZIKV-infected mice, GC B cells specific for NS1 were readily detected at relatively high frequencies (Fig. 3 F). The proportion of GC B cells reacting to NS1 (4.5%) was 10-fold higher than that of GC B cells binding to envelope proteins (0.4%; Fig. 3 G) and correlated with virus-specific IgG levels observed in serum (Fig. 3 C; see also Fig. 1, F and I). These findings underscore the extent of the immunodominance of NS1 over envelope antigens also at the cellular level.

We then performed the global analysis of self-reactivities, as used for serum IgG (Fig. 2 H), with GC B cell culture supernatants.

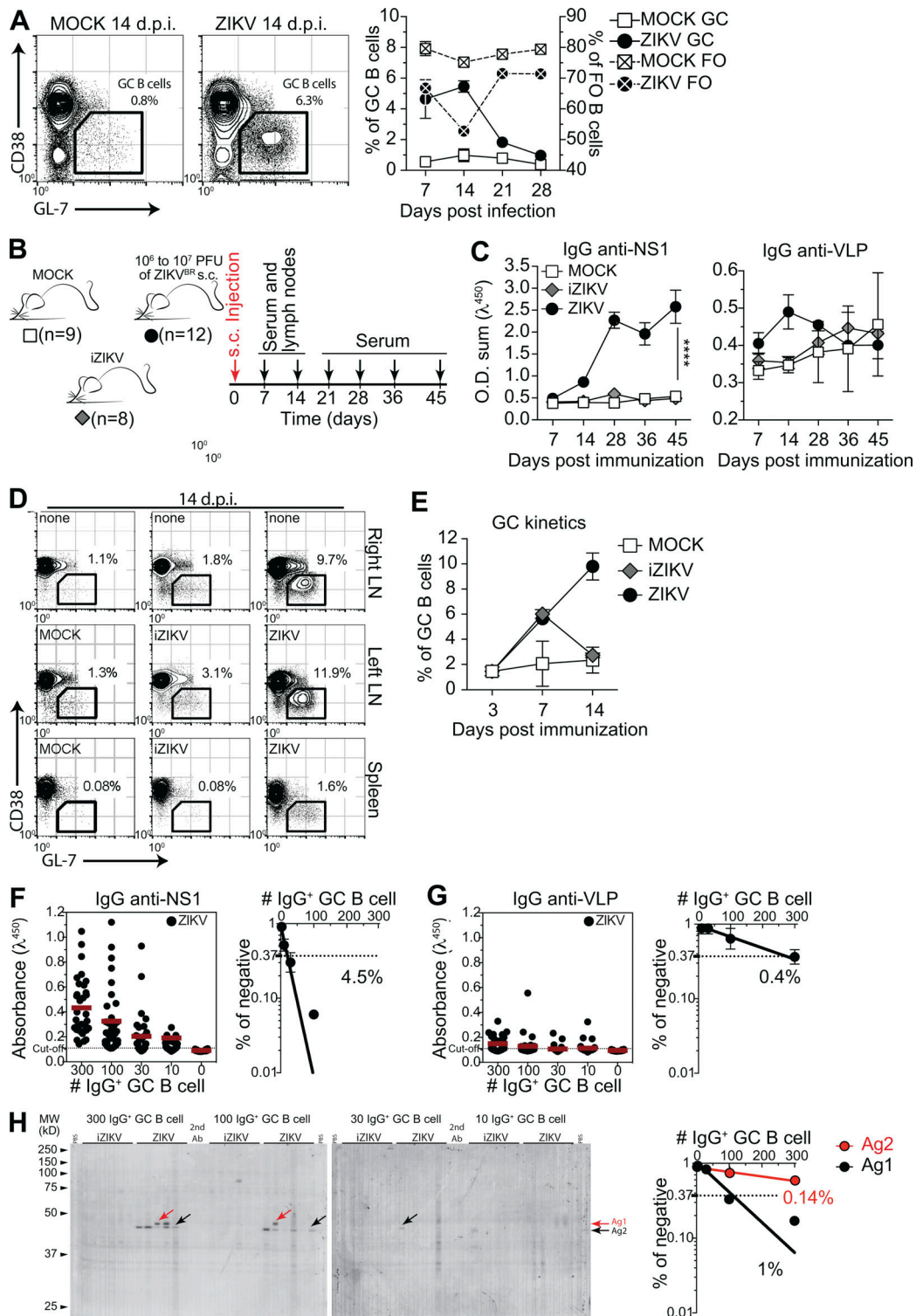


**Figure 3. GC B cells produce both virus-specific and autoreactive antibodies.** (A) GC B cells (CD38<sup>lo/-</sup> GL-7<sup>+</sup> gated on B220<sup>+</sup> CD138<sup>-</sup>) in the spleen of ZIKV-infected mice at 14 d.p.i. (left). Kinetics of frequencies of FO and GC B cells after infection (right). (B) s.c. infection experimental design indicating the time points of serum samples and lymphoid tissue collections from control mice (MOCK), mice immunized with UV-iZIKV, and infected mice (ZIKV). (C) Kinetics of serum IgG specific to ZIKV NS1 and VLPs. O.D. sum is the summation of ODs of four serum dilutions (1:40, 1:120, 1:360, and 1:1,080). Statistical analyses were performed using two-tailed Student's *t* test. \*\*\*\*\*, *P* ≤ 0.0001. (D) Representative plots of GC B cells (CD38<sup>lo/-</sup> GL-7<sup>+</sup> gated on B220<sup>+</sup> CD138<sup>-</sup>) at day 14 after infection. Mice were injected in the left footpad. (E) Kinetics of frequency of GC B cells in left popliteal LNs after infection (ZIKV) or immunization (iZIKV). (F–H) GC B cells from popliteal LNs of infected mice were sorted, pooled, and cultured in decreasing numbers per well (300, 100, 30, and 10 cells per well). Supernatants were collected on day 7 and screened for IgG secretion by ELISA. Supernatants that revealed the presence of IgG were tested for antigen specificity by ELISA (F and G) or immunoblot against mouse brain tissue as source of self-antigens (H). Frequencies of IgG<sup>+</sup> GC B cells that bound NS1 (F), VLP (G), or self-antigens (H) were calculated using Poisson distribution. Self-antigen reactivities used for frequency determination are indicated by arrows (antigen 1, black;

antigen 2, red). Cell culture was performed on a monolayer of gamma-irradiated (20 Gy) NB21 feeder cells (Kuraoka et al., 2016;  $3 \times 10^3$  cells/well) and LPS (30  $\mu\text{g/ml}$ ). Ab, antibody; AG, antigen; MW, molecular weight. Data for A are from one experiment representative of two independent experiments with 8–16 mice per group. Data for D and E are from one experiment representative of two independent experiments with six to nine mice per group. Data for F and G are from one experiment representative of two independent experiments with three mice per group. Data for H are from a single experiment with three mice per group. GC B cells were pooled in culture. Error bars represent SEM.

By combining limiting dilution and immunoblot assays, we were able to estimate the frequency of cells secreting IgG binding to self-antigens in each GC B cell culture (Fig. 3 H). Autoreactive B cells were present within GCs formed after exposure to replicative ZIKV, whereas these were virtually absent upon exposure to UV-inactivated virus (Fig. 3 H). Importantly, the self-reactivity found with highest frequency (Ag2) accounted for 1% of GC B cells in the LN (Fig. 3 H), at least twice the frequency of GC B cells detectably specific for virus envelope proteins (Fig. 3 G). These data suggest a role for NS1 in triggering the autoreactive antibody response following ZIKV infection.

### ZIKV NS1 immunization recruits a high frequency of NS1-specific B cells to the GC

To directly test whether an anti-NS1 humoral immune response generates autoreactive antibodies, we immunized mice in the footpad with purified recombinant ZIKV NS1 in the presence of a TLR7 agonist (R848). For comparison, other cohorts of mice were immunized with ZIKV VLPs, displaying envelope proteins (E and M) in the presence of R848 or with a combination of VLPs and NS1 (Fig. 4 A). Analysis of the humoral immune response against the viral antigens revealed that from day 14 after immunization onwards, serum levels of NS1-specific IgG were higher than those of VLP-specific IgG in both combinations (Fig. 4 B). Despite the similar frequencies of total GC B cells in popliteal LNs (Fig. 4 C), frequencies of specific B cells within GCs varied. At day 14 after immunization with VLP/R848, the frequency of GC B cells binding to VLP was 2.6% (Fig. 5 E, left panels). After immunization with NS1/R848, however, the frequency of specific GC B cells was ~10-fold higher, at 27% (Fig. 4 E, right panels). Compared with the single-antigen immunization protocol, VLP and NS1 in combination reduced the frequency of GC B cells specific for both antigens to 1.2% and 3%, respectively (Fig. 4 E, middle panels). This reduction was not due to lower secretion of IgG in vitro, since similar levels of NS1 specific IgG were found in culture supernatants, irrespective of the presence of VLP in the immunization (Fig. 4 F). Altogether, antigen-specific GC B cell frequency and kinetics in immunized mice mirrored the virus-specific IgG levels found in the ZIKV infection model, corroborating the observed immunodominance of NS1 over ZIKV envelope antigens.

### Paucity of SHMs in expanded GC B cell clones from ZIKV NS1-immunized mice

To further characterize the B cell response to ZIKV NS1, we sorted single GC B cells from popliteal LNs of immunized mice at different time points and performed *Igh* sequencing. To gain insight into specific features of ZIKV NS1 B cell response, we also immunized mice with DENV NS1 for comparison. Even though the two proteins are structurally homologous, serum antibodies

generated after infection with ZIKV did not cross-react with DENV NS1 (see Fig. 2 F). As expected, GCs found in popliteal LNs of mice immunized with either ZIKV or DENV NS1 proteins 10 d after immunization were highly clonally diverse, whereas clones with increased frequency accumulated over time (Fig. 5 A).

Analysis of  $V_H$  segment usage showed preferential use of the  $V_{H1}$  (J558) gene family, irrespective of immunizing antigen and time point analyzed (Fig. S4 A). The average number of mutations in  $V_H$  gene segments was similar for both antigens and increased over time as one would expect. However, interestingly,  $V_H$  mutation numbers were lower among clones found more frequently (likely those undergoing positive selection) in GCs formed after ZIKV NS1 immunization when compared with those formed after DENV NS1 immunization (Fig. 5 B). B cells in GCs from DENV NS1-immunized mice tended to progressively accumulate mutations in more expanded clones over time (Fig. 5 C).

Although no significant differences in CDR-H3 length were found in GC B cells after DENV or ZIKV NS1 immunization at any time point (Fig. S4 B), there was a preference for 11-amino acid-long CDR-H3s in both ZIKV NS1- and DENV NS1-immunized mice when compared with the naive B cell repertoire (Fig. S4 C). Average CDR-H3 hydrophobicity tended to be lower for ZIKV NS1 than for DENV NS1 (Fig. 5 D). The distribution of CDR-H3 average hydrophobicity revealed few highly charged sequences among B cells responding to ZIKV NS1 antigen (Fig. 5 E). Comparison of the amino acid composition of CDR-H3 regions at different time points revealed an enrichment over time for charged amino acids, especially arginine after ZIKV NS1 immunization (Fig. 5 F). Of note, charged amino acids in the antigen-binding sites of IgG are often critical for self-reactivity (Radic et al., 1993). However, a marked glycine (neutral amino acid) enrichment was also observed, which could counterbalance the charged amino acid bias, resulting in a moderate change in average hydrophobicity in CDR-H3 as shown in Fig. 5 D. Evaluating the percent difference between hydrophobic and charged amino acids in CDR-H3 sequences, we found that B cell clones derived from ZIKV NS1-immunized animals used charged amino acids more frequently than hydrophobic ones when compared with the DENV NS1-immunized mice (Fig. 5 G).

The recruitment of B cells enriched in charged CDR-H3 amino acids into GCs upon immunization with ZIKV NS1 could be related to the emergence of autoreactive IgG. Although, the specificities of the Igs encoded by these sequences are not known, results obtained with GC B cell cultures suggest that most of these cells (63% for ZIKV NS1 and 97% for ZIKV VLP) do not secrete antibodies with detectable binding to the immunizing antigen (see Fig. 4 E). One might expect that the most expanded clones would be those with the greatest affinity for the

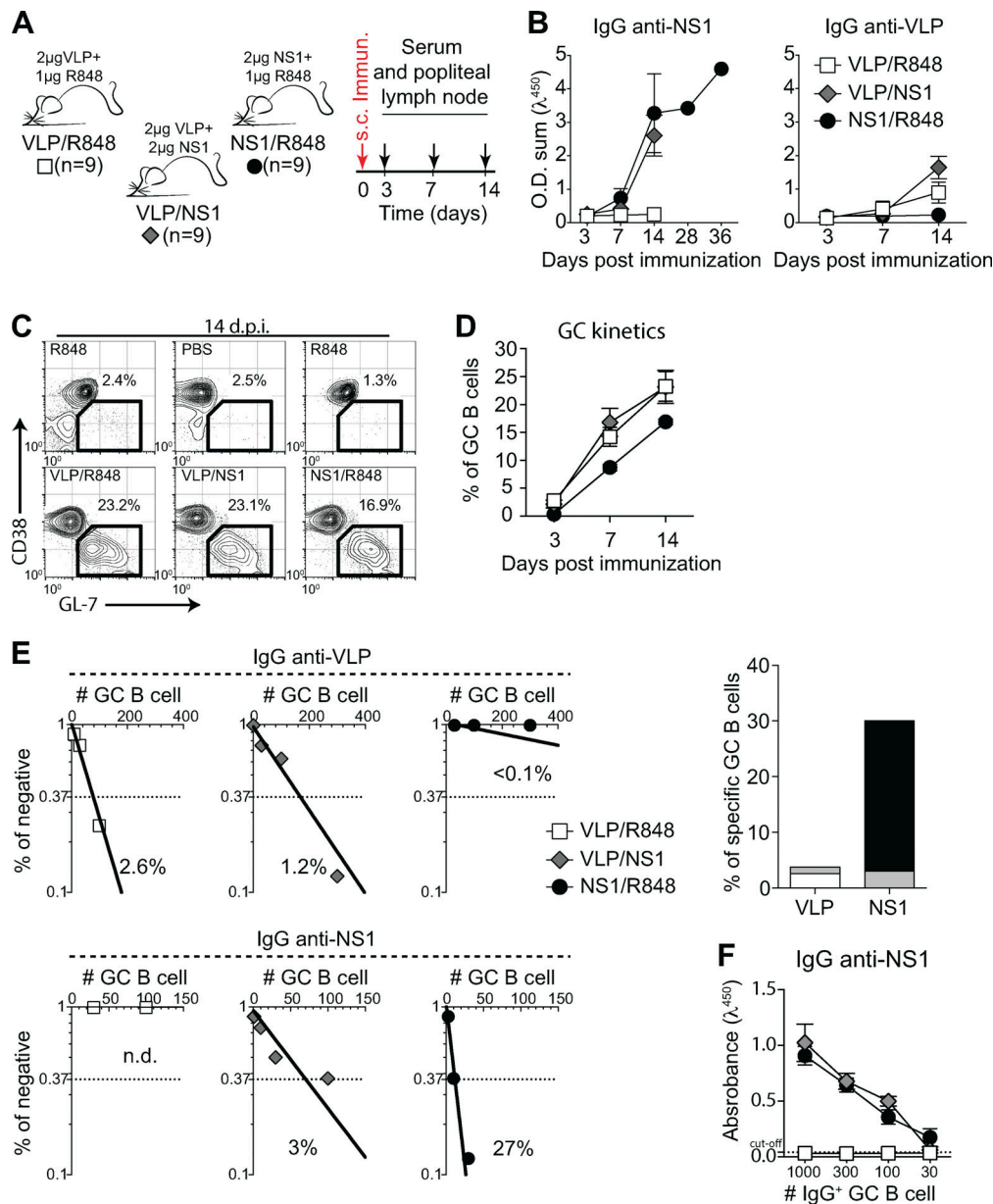


**Figure 4. Antigen specificity of B cells in GCs after immunization with ZIKV VLP and NS1.** (A) Experimental design indicating the time points of serum samples and popliteal LN collections after immunization with NS1 (2  $\mu$ g/mouse), VLP (2  $\mu$ g/mouse) or both (2  $\mu$ g of NS1 and 2  $\mu$ g of VLP/mouse). Immunizations were adjuvanted with R848 (1  $\mu$ g/mouse). (B) Kinetics of serum levels of IgG binding to ZIKV NS1 recombinant protein or ZIKV VLP, measured by ELISA. O.D. sum is the sum of ODs of four serum dilutions (1:40, 1:120, 1:360, and 1:1,080). (C) Representative plots of GC B cells (CD38<sup>lo/-</sup> GL-7<sup>+</sup> gated on B220<sup>+</sup> CD138<sup>-</sup>) at day 14 after immunization. Mice were immunized on the left footpad. (D) Kinetics of frequency of GC B cells in left popliteal LNs after immunization. (E) GC B cells from popliteal LNs of immunized mice were sorted and cultured in decreasing numbers per well (300, 100, 30, and 10 cells per well). Supernatants were collected on day 7 and screened for IgG secretion by ELISA. Supernatants that revealed the presence of IgG were tested for antigen specificity by ELISA. Frequencies of IgG<sup>+</sup> GC B cells that bound VLP (upper panel) or NS1 (lower panel) were calculated using Poisson distribution and are summarized on the right graph. n.d., not detected. Cell culture was performed on a monolayer of gamma-irradiated (20 Gy) NB21 feeder cells (Kuraoka et al., 2016;  $3 \times 10^3$  cells/well) and LPS (30  $\mu$ g/ml). (F) OD of IgG<sup>+</sup> supernatants of different cell numbers/well binding to ZIKV NS1, measured by ELISA. Data are representative of two independent experiments with nine mice per group. Error bars represent SEM.

antigen; however, it remains possible that the most mutated clones would expand at later time points, after more extensive selection, and would therefore not be detected at high frequencies in the samples we analyzed. To better understand this phenomenon, we sought to correlate the features of Ig variable gene sequences with the specificities of their secreted antibodies.

**ZIKV NS1 immunization recruits into GCs B cell clones enriched for charged amino acids in the CDR-H3s and self-reactivity**

To understand the relationship between Ig sequence features and antigen specificity, we used single GC B cell cultures, which allow the assessment of both *Igh* sequence and binding properties from the same cell (adapted from Vale et al., 2012). For this purpose, GC B cells were harvested from popliteal LNs of mice

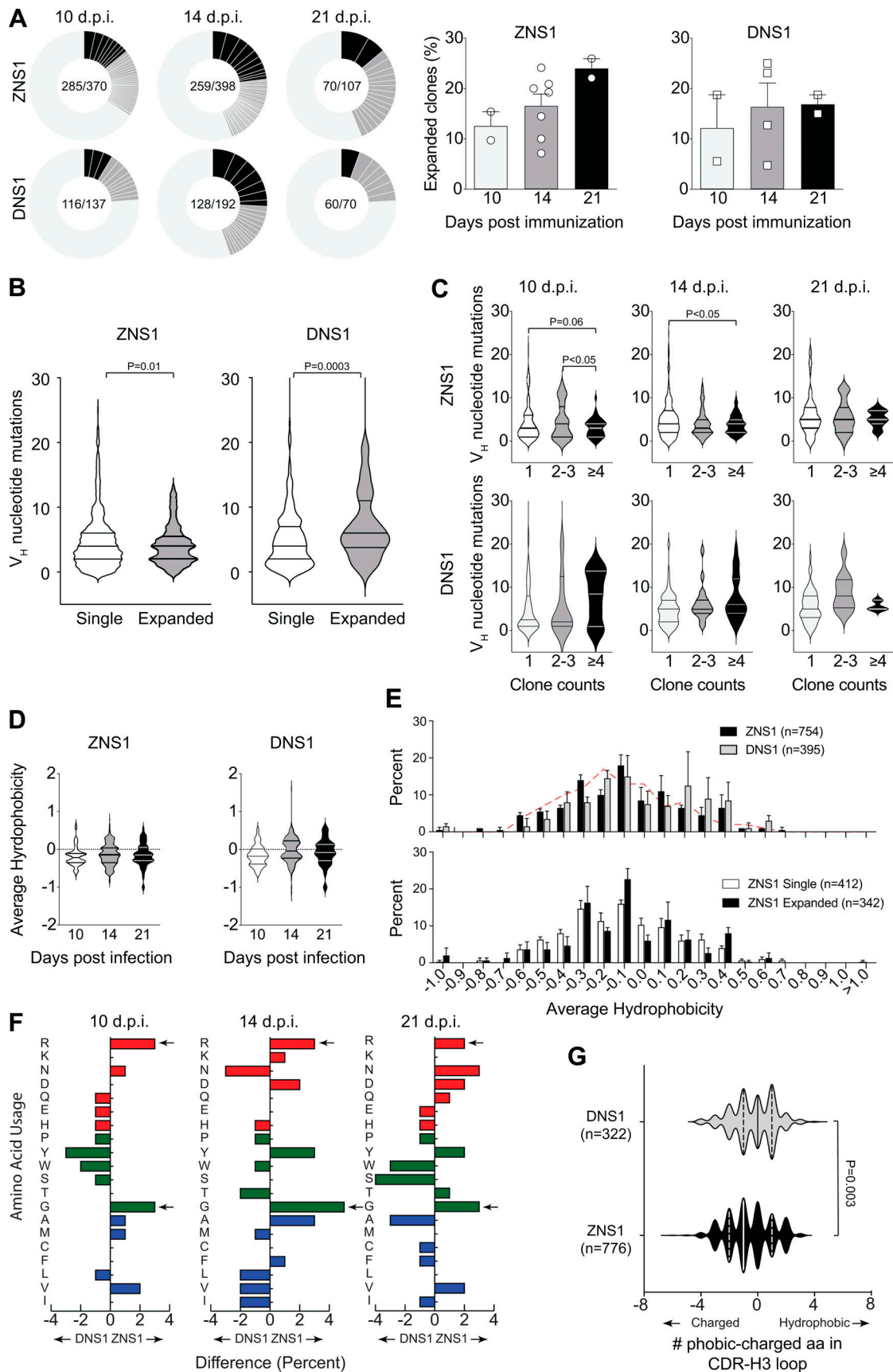


Figure 5. **Characterization of B cell repertoire present in GCs after ZIKV NS1 immunization.** (A) Single GC B cells from mice immunized s.c. with recombinant ZIKV NS1 or DENV NS1 were sorted at indicated time points after immunization, and *Igh* gene was sequenced. Pie charts represent clonal diversity

found in all LNs analyzed. Slices represent clonotypes assigned based on  $V_H$  and  $J_H$  usage and CDR-H3 length and sequence. Slice size is proportional to the frequency of each clone. Black slices indicate clone counts higher than four. Dark gray slices indicate clone counts of two or three. Light gray where slices are not delimited represents single clones. Proportion of expanded clones is indicated on the right. **(B)** Number of somatic mutations found in  $V_H$  segments separated by singletons versus expanded clones. **(C)** Number of somatic mutations found in  $V_H$  segments at different time points separated by clone count. **(D)** CDR-H3 average hydrophobicity index variation among all sequences at indicated time points after immunization. **(E)** Comparison of CDR-H3 average hydrophobicity index distribution among all sequences from mice immunized with ZIKV NS1 or DENV NS1 (upper panel) and comparison between expanded (clonotypes found more than once in the same LN) and single clones from mice immunized with ZIKV NS1 (lower panel). Dashed red line indicates the distribution of CDR-H3 average hydrophobicity in FO B cells from WT BALB/c mice. The normalized Kyte–Doolittle hydrophobicity scale (Kyte and Doolittle, 1982) was used to calculate average hydrophobicity. **(F)** Divergence in the distribution of individual amino acid usage in the CDR-H3 loop between ZNS1- and DNS1-immunized mice at each time point. Red bars indicate charged amino acids, green bars represent neutral amino acids, and blue bars represent hydrophobic amino acids. Arrows indicate enrichment in arginine (R) and glycine (G) in ZIKV NS1 CDR-H3 loops. **(G)** Difference in number of hydrophobic and charged amino acids among all sequences from DENV NS1-immunized mice (gray) and ZIKV NS1-immunized mice (black). GC B cells were sorted and sequenced from individual LNs and pooled for analyses (two to four mice per group from two independent experiments). Statistical analyses were performed using the unpaired two-tailed Student's *t* test. Error bars represent SEM.

immunized with ZIKV or DENV-NS1 protein at different time points after immunization. After 7 d in culture, cells were processed for *Igh* sequencing, and supernatants were used for specificity assessment. We first determined the frequency of GC B cells secreting ZIKV NS1-binding IgG. A total of 271 monoclonal antibodies were tested for binding to NS1 protein. In line with the rising levels of serum IgG specific for NS1 (shown in Fig. 4 B), frequency of ZIKV NS1-specific B cells also increased over time, from an average of 30% at 10 d.p.i. to 50% at 21 d.p.i. (Fig. 6 A). We then divided B cell clones into NS1 binders and nonbinders for further analyses. Clonal expansion was evident among NS1-binding GC B cells, peaking on day 14 after immunization (when almost 60% of NS1 binders were found in detectably expanded clonotypes), consistent with antigen-driven selection (Fig. 6 B). At 21 d.p.i., the fraction of expanded clones among NS1 binders decayed to a frequency similar to that found at day 10 after immunization. Although the number of clones analyzed at this time point is limited, this result could suggest continued ingress of new B cell clones into ongoing GCs (Fig. 6 B). In contrast, nonbinder clones showed significantly less clonal expansion at all time points analyzed (Fig. 6 B). Interestingly, and consistent with data shown previously (Fig. 5 B), we did not find evidence for positive selection of NS1-binding clones bearing large numbers of somatic mutations (Fig. 6 C).

We then investigated the physicochemical features of the CDR-H3 sequences expressed by B cells recruited to GCs after ZIKV NS1 immunization. On day 14 after infection, both ZIKV NS1 binders and nonbinders showed similar CDR-H3 hydrophobicity, whereas on day 21 after infection, ZIKV NS1 binders tended to be less charged and closer to neutrality than nonbinders, an effect just short of statistical significance (Fig. 6 D). To examine whether NS1 binding correlated with the abundance of positively charged amino acids in CDR-H3, we plotted the anti-NS1 reactivity per clone at each time point, highlighting CDR-H3s expressing three or more charged amino acids (Fig. 6 E, red dots). CDR-H3s bearing charged amino acids were frequent and evenly distributed among NS1 binder and nonbinder clones, accounting for 25–35% of CDR-H3 sequences (Fig. 6 E). Overall, CDR-H3s of GC B cells from ZIKV NS1-immunized mice were enriched for charged amino acids (including arginine), as compared with what has been observed in the naive repertoire (Ivanov et al., 2005), as well as in comparison to clones from DENV NS1-immunized mice (Fig. 5, F and G; and Fig. 6 E).

The presence of positively charged amino acids within CDR-H3 is a common feature associated with self-reactivity (Radic and Weigert, 1994). To determine whether particular *Igh* sequence features were correlated with self-reactivity, we tested 72 monoclonal antibodies for binding to autologous muscle and brain extracts (Fig. 6 F and Table S1). In accordance with the results obtained with serum and limiting dilution of GC B cells, no self-reactivity was found among GC B cells from DENV NS1-immunized mice at any time point (Fig. 6 F and Table S1). In contrast, 18.2% of evaluated single cells obtained at day 14 after immunization with ZIKV NS1 were self-reactive. This frequency increased to 42.3% of the analyzed cells from 21 d.p.i. Highly charged CDR-H3 was not determinant for self-reactivity, since we found this feature among both self-reactive and non-self-reactive clones. Nevertheless, we did find a handful of clonotypes bearing hydrophobic amino acids in their CDR-H3 that were predominantly self-reactive (Fig. 6, F and I; and Table S1).

To further investigate the specific association of ZIKV NS1 with autoreactivity, we performed limiting dilution assays and single-cell cultures with GC B cells isolated from mice immunized with OVA, as an irrelevant antigen. As with DENV NS1, no self-reactivity was observed among GC B cells derived from OVA-immunized mice (Fig. S5).

#### GC B cells from ZNS1-immunized mice display widespread self-reactivity irrespective of clonal sizes, SHM and nominal antigen-selection

We further analyzed the SHM patterns and clonal frequencies of those GC B cells for which we obtained a complete dataset, correlating it with IgG reactivity to NS1 and to self-antigens. Among GC B cells obtained at day 14 after immunization with ZIKV NS1, we found cells with similar CDR-H3 but different SHM patterns, including a clonal family bearing a “glycine-enriched CDR-H3” (ARGGGYDGFAY). The least mutated cell in this group was inferred to have acquired a nonsilent mutation in the D2-02 gene segment, which led to the replacement of a tyrosine by a phenylalanine in the CDR-H3 (becoming ARGGGFDGFAY). The germline D2-02 D gene segment encodes the GYD motif, whereas the mutated version encoded a GFD motif, which displayed increased polyreactivity against self-antigens together with increased reactivity to ZNS1 (Fig. 6 G and Table S1). The two clones bearing the glycine-enriched CDR-H3 that bound NS1 and cross-reacted with self-antigens were also

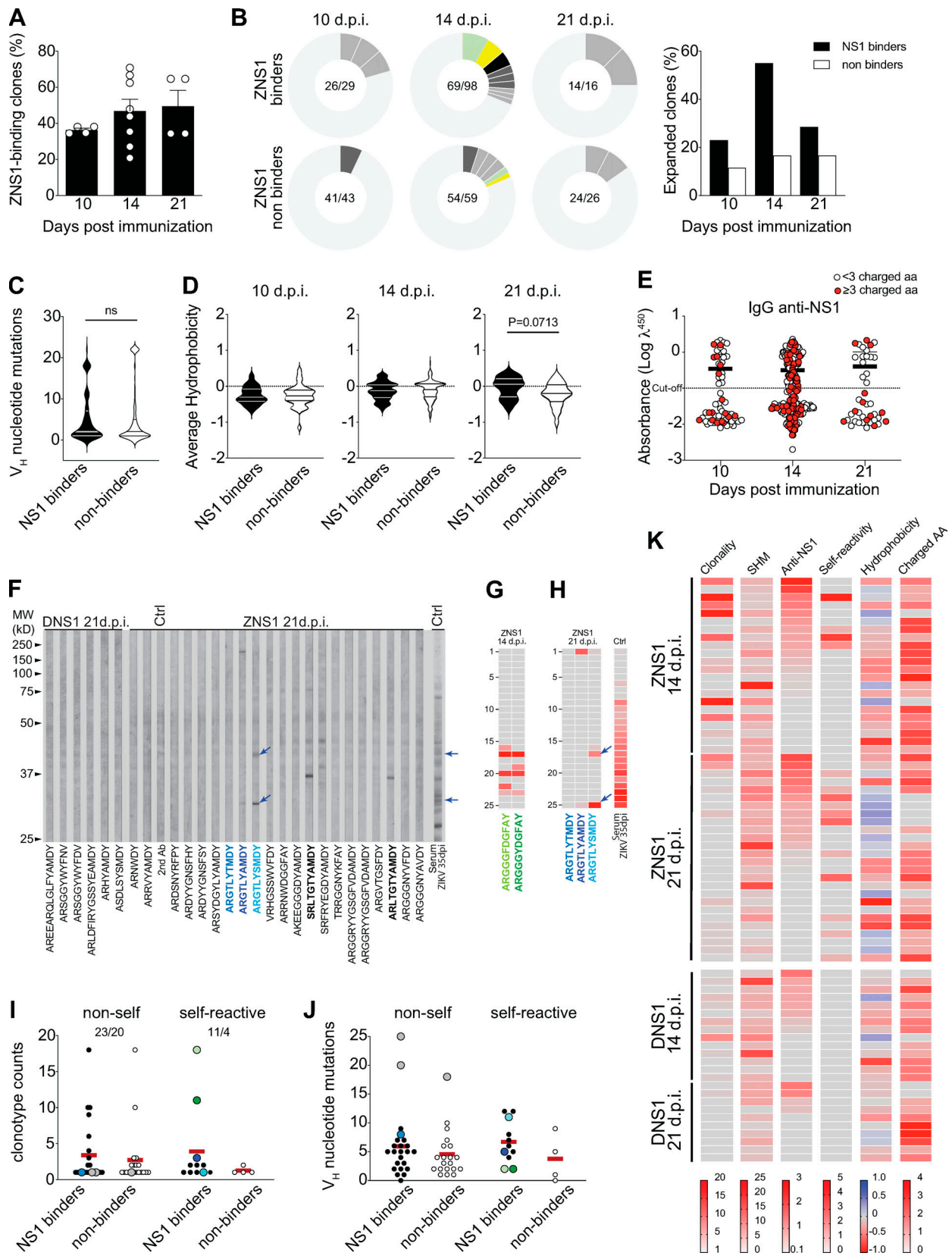


Figure 6. **Self-reactivity of GC B cells after ZIKV NS1 immunization.** Single GC B cells were sorted and cultured on a monolayer of gamma-irradiated NB21 feeder cells ( $10^3$  cells/well; Kuraoka et al., 2016). After 7 d, supernatants were collected for binding assays, and cells were harvested for *Igh* sequencing. (A) Frequency of IgG<sup>+</sup> single GC B cell culture supernatants that bound to ZIKV NS1 per LN. IgG<sup>+</sup> wells were tested for binding to ZIKV NS1 protein by ELISA. (B) Clonal distribution of GC B cells found to bind to NS1 (upper panel) or that did not bind to NS1 (lower panel). Size of the slice is proportional to the clone

frequency. Colored slices represent variants of clones that were found both as binders and nonbinders. Right panel represents the frequency of expanded clones among binders and nonbinders at specific time points after immunization. **(C)** Number of somatic mutations found in  $V_H$  segments from each GC B cell sequenced grouped based on binding to NS1. **(D)** CDR-H3 average hydrophobicity index variation at different time points grouped by binding to NS1. Statistical analyses were performed using the unpaired two-tailed Student's *t* test. **(E)** NS1 binding by ELISA OD related to the presence of charged amino acids. Red dots indicate the presence of three or more charged amino acids in CDR-H3 at different time points. **(F–I)** Single GC B cell culture supernatants were tested for binding to self-antigens by immunoblot. **(F)** Representatives immunoblot profiles of monoclonal IgG from single GC B cell culture supernatants binding to mouse brain extract. Arrows indicate immunoreactivities highlighted in the main text. **(G)** Immunoreactivity profile of two poly-reactive variants from the clonal family bearing “glycine-enriched CDR-H3” (ARGGGYDGFAY) found among GC B cells from mice 14 d.p.i. with ZIKV NS1. **(H)** Immunoreactivity profile of the autoreactive clonotype ARGTLYAMDY and its two more mutated variants, ARGTLYTMDY (nonautoreactive) and ARGTLYSMDY (autoreactive). **(I)** Clonotype counts of NS1 binders (black dots) and NS1 non binders (white dots) separated by self-reactivity. Color-coded dots represent variants of clones described in the main text. **(J)** Number of somatic mutations found in  $V_H$  segments grouped by binding to NS1 and self-reactivity. Color coded dots represent variants of clones described in the main text. **(K)** Clonality, SHM, binding to NS1, self-reactivity, hydrophobicity, and charged amino acid usage by time after immunization. Clonality corresponds to the number of variants of each clonotype found in the dataset. SHM is represented by the number of  $V_H$  mutations found in each sequence. Anti-ZNS1 indicates the OD obtained by ELISA. Self-reactivity corresponds to the number of bands found for each supernatant in mouse tissue extracts (brain and/or muscle). Hydrophobicity corresponds to the average hydrophobicity of the CDR-H3 loop, and hydrophobic and charged CDR-H3 sequences are shown in blue and red, respectively. Charged AA indicates the number of charged amino acids found in the CDR-H3 loop. GC B cells were sorted and sequenced from individual LNs and pooled for analyses (two to four mice per group from two independent experiments). Error bars represent SEM.

highly expanded, suggesting that antigen-specific GC B cells, whether self-reactive or not, are capable of undergoing positive selection (Fig. 6 I, green dots).

At 21 d.p.i., other groups of related clonotypes were found with different SHM patterns (Fig. 6 F and Table S1). An interesting autoreactive clone carried the ARGTLYAMDY CDR-H3 (Fig. 6 F, highlighted in blue). In addition to being among the most hydrophobic sequences in our list, we found more mutated variants both nonautoreactive (ARGTLYTMDY) and autoreactive (ARGTLYSMDY; Fig. 6, F and H; and Table S1). Although all variants of this clonal family bound to ZIKV NS1 protein, the most mutated one (ARGTLYSMDY) displayed the highest relative reactivity to NS1 (Table S1) as well as increased poly- and self-reactivity (Fig. 6, F and H, highlighted in light blue). In this case, only the least mutated sequence (ARGTLYAMDY) was found more than once in the dataset. Notably, the two most prominent self-reactivities found in the ARGTLYSMDY clone were also found in serum from infected mice at 35 d.p.i. (Fig. 6, F and H, arrows).

ZIKV NS1 clonotypes found at the highest frequencies (>5 counts) were generally non-self-reactive (Fig. 6 I). Moreover, all NS1-binding Igs tested for self-reactivity, regardless of their self-reactivity status, had numbers of  $V_H$  mutations that were similar and higher than those of non-antigen-specific cells, again suggesting antigen-driven selection (Fig. 6 J). The most mutated clones did not bind to self-antigens and were found exclusively as singletons, irrespective of binding to ZIKV NS1 (Fig. 6, I and J, gray dots).

The results obtained with single-cell sequencing and binding assays were summarized in Fig. 6 K. Clonality scores showed that the presence of more expanded clones was a property of earlier GCs, obtained at 14 d.p.i., whereas late GCs were enriched in smaller clones. Self-reactive clones were already present at day 14, all of which exhibited cross-reactivity with ZIKV NS1. Interestingly, autoreactive clones with no cross-reactivity with NS1 were present at 21 d.p.i. but not at 14 d.p.i. Although the number of clones assayed for autoreactivity limits the strength of this conclusion, we found more self-reactivity among NS1 binders than among nonbinders. Collectively, our data support a role for NS1 in recruiting cross-reactive B cell clones into GCs,

some of which are self-reactive clonotypes showing evidence for clonal expansion and paucity of  $V_H$  gene mutations.

## Discussion

Mice are not a natural host for ZIKV, and immunodeficient mouse models have been preferred for pathogenesis studies (Lazear et al., 2016; Bardina et al., 2017; Dowall et al., 2016). However, while pathological studies are better characterized in these experimental models, they are less useful for the analysis of humoral immune responses. Here, we have established a ZIKV infection model in immunocompetent BALB/c mice to study the normal humoral immune response. Human and mouse immune responses to ZIKV infection very likely differ, but their consequences for the generation of antibodies to virus antigens are not known. The humoral immune response to ZIKV infection in humans is characterized by early appearance of antibodies to structural proteins of the viral envelope followed by later increase in antibodies to the nonstructural protein NS1 (Gao et al., 2018; Stettler et al., 2016). However, we found that the humoral immune response of immunocompetent BALB/c mice to ZIKV infection follows a similar pattern. Other common features of the human humoral response were also observed, such as kinetics and cross-reactivity of EDIII-binding antibodies with DENV EDIII, but not of NS1-specific antibodies. Even though, in our study, mice were either infected i.v. or s.c., thus not via the natural route of infection through mosquito bites, which could influence the immune response through components present in the saliva. The BALB/c antibody response is characterized by early emergence of envelope-specific IgG, including EDIII-specific and neutralizing antibodies, followed by a delayed response dominated by antibodies to NS1. The delayed response to NS1 may be a consequence of its absence from the viral particle, possibly explaining the initial dominance of anti-envelope antibodies. Only after productive ZIKV infection do cells start producing and secreting large amounts of NS1, which then accumulates in bodily fluids and on the surface of infected cells. NS1 circulates in blood and has been implicated both in damage to endothelial cells and in immune evasion through inhibition of the complement cascade (Reyes-Sandoval and

Ludert, 2019; Avirutnan et al., 2010; Puerta-Guardo et al., 2019; Conde et al., 2016). Of note, antibodies to NS1 have been shown to be protective against Zika and dengue diseases, and immunization with NS1 has been considered as a possible prophylactic strategy (Modhiran et al., 2021; Beatty et al., 2015; Bailey et al., 2019).

Antibodies to DENV NS1 have also been implicated in pathological autoreactivity in humans (Chuang et al., 2016; Cheng et al., 2009). From this perspective, it is interesting to note that reactivity toward self-antigens was observed in the humoral immune response of BALB/c mice to ZIKV infection. We evaluated reactivities to different tissues and cell extracts, including a human cell line extract, which suggests that self-reactivity triggered by ZIKV infection can target possibly common epitopes in different species. The presence of autoreactive antibodies in viral diseases is not an uncommon finding and is often attributed to nonspecific polyclonal B cell activation. ZIKV infection has been associated with Guillain-Barré syndrome in which anti-ganglioside antibodies have been shown to play a role. Although we have not searched for these antibodies, it is worth noting that other antigens of the myelin sheath have been suggested to trigger demyelination and neuropathy in a T cell-dependent manner (Csurhes et al., 2005); in this scenario, B cells would mostly play the role of antigen-specific antigen-presenting cells (Molnarfi et al., 2013). Our data support the notion that self-reactivity with brain derived antigens is already present in the early GC reaction to NS1 antigen, which could be a mechanism underlying brain tissue attack by the immune system in a percentage of ZIKV-infected individuals. This targeted B cell recruitment and activation stands in contrast with the notion of bystander polyclonal B cell activation. Whether these findings can be translated into understanding the ZIKV-associated human disease certainly deserves further investigation.

Autoreactive B cells can be stimulated in a T cell-independent manner as well via simultaneous TLRs and BCR signaling both in GCs and in extrafollicular foci (Akkaya et al., 2018; Bessa et al., 2010; Das et al., 2017; Degn et al., 2017). However, polyclonal B lymphocyte activation is mostly an acute phase phenomenon that subsides with clearance of the virus. Here, by contrast, we found that self-reactivity was sustained and even augmented at later time points after infection, long after ZIKV had been eliminated. Interestingly, NS1-specific antibodies were also long-lasting in serum and correlated well with the kinetics of appearance and maintenance of autoreactive antibodies in BALB/c mice. Serum IgG isotypes composition of the NS1-specific repertoire was coherent with the sustained IgG anti-NS1 response and the engagement of new clonotypes. Early predominant IgG2a response was followed by a later emergence of IgG1, while IgG2a titers still increased up to 50 d.p.i. As sequential switching from IgG2a to IgG1 is not a possibility, this result implicates the recruitment of new clones to sustain anti-NS1 antibody levels. It is still not clear whether the response to the viral antigen is maintained by self-antigens or the viral antigen itself, which could be present at later time points, even though the virus was not detected after the first week of infection, as long-term antigen persistence in FO dendritic cells has been well documented (Heesters et al., 2014). Interestingly,

at the GC level, the decrease in clonal dominance between days 14 and 21 after NS1 immunization inversely correlated with increased self-reactivity, corroborating the possibility of replacement of early clones with a new wave of B cells with self-reactive potential. SHM appeared not to increase from day 14 to 21, which would also be in line with clonal replacement. Hence, the kinetics of the NS1 response is unique and differs from that induced by viral surface antigens, progressively dominating the humoral response. The shift from anti-envelope to anti-NS1 response could be a viral escape strategy, since neutralization is achieved mostly by antibodies directed to viral surface proteins. Additionally, since NS1 plays a role in pathogenesis, promoting endothelial dysfunction and increasing vascular permeability (Puerta-Guardo et al., 2019; Beatty et al., 2015; Modhiran et al., 2015), it is also possible that the systemic effects of this protein may skew the immune response toward it contributing to protection (Modhiran et al., 2021; Bailey et al., 2019). However, this protective response might develop at the cost of the production of self-reactive antibodies that could contribute to autoimmune manifestations related to infection, as previously mentioned.

Our analysis of GC B cells from ZIKV-infected mice revealed both virus-specific and self-reactive B cells. Using single-cell cultures of GC B cells from mice immunized with ZIKV NS1, we showed that both anti-NS1 and autoreactivity could often be attributed to the same cell. It is worth noting that the presence of autoreactive IgG in serum after ZIKV infection and of self-reactive B cells within GCs of NS1-immunized animals does not directly demonstrate that these cells will automatically be licensed to become long-lived plasma cells. Whether additional post-GC checkpoints play a role in preventing these cells from differentiating into plasma cells requires further investigation. Although GC responses to ZIKV NS1 and DENV NS1 did not differ in kinetics and were of short duration, autoreactive clones were found at all time points investigated after ZIKV NS1 immunization, but not after DENV NS1 or OVA immunization. As previously mentioned, serum IgG anti-ZIKV NS1 did not cross-react with DENV NS1, in agreement with the distinct reactivity profiles reported here.

Self-reactive antibodies associated with autoimmune diseases, such as lupus, have been shown to be enriched for charged amino acids, especially arginine, in CDR-H3 (Radic and Weigert, 1995). Under normal circumstances, immunocompetent BALB/c mice are considered resistant to production of these autoantibodies (Sekiguchi et al., 2006; Silva-Sanchez et al., 2015). This is in part due to the low prevalence (~5%) of arginine in the CDR-H3 region of the BCRs of mature recirculating B cells in BALB/c mice (Ivanov et al., 2005). Half of the arginines in CDR-H3 regions of immature B cells in BALB/c mice derive from N additions and half from germline  $D_H$  sequences (Silva-Sanchez et al., 2015). Here, we found an enrichment for charged amino acids, including arginine, in CDR-H3 of GC BCRs after ZIKV NS1 immunization, as compared with DENV NS1. Interestingly, one particular clone found at high frequency among GC B cells at day 14 after immunization with ZIKV NS1 used the D gene segment DSP2.11 (D2-14), the only one to encode arginine in the germline sequence in reading frame 1 (Silva-Sanchez et al., 2015). Notably,

a marked glycine enrichment in CDR-H3 was also observed, which might contribute to maintaining the average hydrophobicity close to neutrality. NS1 is a complex multifunctional protein that forms a peculiar hydrophobic core in its hexameric structure when it is secreted by infected cells (Muller and Young, 2013). Interestingly, in addition to the enrichment for charged amino acids, we also found self-reactive clonotypes bearing hydrophobic CDR-H3s; whether these particular clonotypes are able to bind to hydrophobic epitopes on NS1 protein, revealing potential immunogenicity of this hydrophobic core, remains to be determined.

*Igh* sequencing of B cells isolated from GCs of ZIKV NS1- or DENV NS1-immunized mice showed similar usage of  $V_H$  segments and similar average number of  $V_H$  mutations, increasing over time as one would expect. However, after ZIKV NS1 immunization,  $V_H$  mutation numbers were lower among clones found more frequently, possibly indicating selection of near-germline B cell clones. We speculate that this could be due to the availability, in the preimmune repertoire, of B cells able to bind to ZIKV NS1 protein with enough affinity to differentiate rapidly into plasma cells before accumulating many mutations. As recently shown by Burnett and colleagues, selection in GCs is skewed toward lower affinity for self-antigens before increasing affinity to foreign antigens (Burnett et al., 2018). In this context, it is possible that anti-ZIKV NS1 clones could generate plasma cells before acquiring enough mutations to diminish affinity to self-antigens. While it is known that plasma cell differentiation in GCs is dependent on high BCR affinity, the mechanisms through which the affinity threshold for differentiation is set are unclear (Tas et al., 2016; Viant et al., 2020).

Coupling sequence analysis to binding assays, we found that NS1-specific B cells had similar numbers of  $V_H$  mutations (higher than those of nonspecific clones), regardless of being self-reactive or not. By contrast, self-reactive B cells that did not bind to ZIKV NS1 protein were the least mutated of all and were also not detectably expanded (Fig. 6, I and J). These data suggested the presence of antigen-driven selection despite self-reactivity, although, among NS1-specific cells, self-reactive B cells seemed disfavored as compared with non-self-reactive ones. For instance, the glycine-enriched CDR-H3 ARGGGYDGFAY likely further mutated to ARGGGFDGFAY, generating increased poly- and self-reactivity while simultaneously increasing its reactivity to ZNS1. The autoreactive clonotype ARGTLYAMDY, on the other hand, was found in further mutated versions, ARGTLYTMDY, which lost autoreactivity, and ARGTLYSMDY, which remained autoreactive (Fig. 6 H and Table S1). Overall, our observations suggest that GC B cell clones undergoing selection after ZIKV NS1 immunization tend to be closer to germline than those in DENV NS1 immunization, an intriguing finding that requires further investigation.

In conclusion, we show here, for the first time, that ZIKV NS1-specific GC B cells can cross-react with self-antigens, possibly by molecular mimicry, raising the question of whether self-antigens can participate in the stimulation of anti-NS1 B cell clones. This hypothesis could explain the sustained progression of the anti-NS1 humoral immune response we observed in infected mice. Notably, autoreactive clones that did not react with

ZIKV NS1 were also found in GCs, presenting the possibility of a “true” break of self-tolerance in the immune response to viral infection that goes beyond antigen mimicry. Finally, the flavivirus NS1 protein has been proven highly immunogenic in humans and capable of inducing protective antibodies and therefore suggested as a potential vaccine antigen (Gonçalves et al., 2015; Bailey et al., 2019) or therapeutic antibody target (Modhiran et al., 2021). In this context, our data call attention to in-depth analysis of B cell clones engaged in response to this viral antigen and the safety of those clinical approaches, especially concerning their autoreactive component. This concern is echoed in very recent studies highlighting the self-reactive potential of near-germline-encoded antiviral antibodies to severe acute respiratory syndrome coronavirus 2, the infectious agent of coronavirus disease 2019 (Andreano and Rappuoli, 2021; Bastard et al., 2020; Andreano et al., 2021; Kreer et al., 2020), arguing that the phenomenon described here may be of importance well beyond the specific case of ZIKV infection.

## Materials and methods

### Mice and treatments

BALB/c adult female WT mice, aged 6–8 wk, were obtained from Federal Fluminense University (Nucleus for Laboratory Animals), Federal University of Rio de Janeiro (Laboratory for Transgenic Animals) or The Jackson Laboratory. Mice were kept in a 12-h light/dark cycle with ad libitum access to food and water. Mice were infected with  $10^6$ – $10^7$  PFUs of ZIKV PE243 (Coelho et al., 2017) i.v. or s.c., as indicated. Lymphoid tissues and blood sample collections are indicated for each experiment. ZIKV strain PE243 (Brazil/South America, GenBank accession no. KX197192) was propagated and titrated in Vero cells and UV inactivated as previously described (Coelho et al., 2017). Immunizations were performed with recombinant DENV NS1 and ZIKV NS1 and ZIKV VLPs expressed as previously described (Conde et al., 2016; Alvim et al., 2019) or OVA (grade V chicken; Sigma-Aldrich). Mice were immunized in the footpad with 2  $\mu$ g/mouse of recombinant protein, VLP, both or OVA adjuvanted with R848 (1  $\mu$ g/mouse). All animal procedures were approved by the Institutional Animal Care and Use Committee of the Centro de Ciências da Saúde da Universidade Federal do Rio de Janeiro and The Rockefeller University.

### ELISA for Ig quantification

Total IgG and IgM concentration in serum and cell culture supernatants were determined by ELISA as previously described (Vale et al., 2010) using anti-mouse IgM- and IgG-specific reagents (Southern Biotechnology). Briefly, 96-well plates (Costar) were incubated with anti-IgM or anti-IgG capturing antibody at 1  $\mu$ g/ml (Southern Biotech) and incubated at 4°C for 18 h. Then, after 1 h of blocking (PBS-BSA 1%), serum samples and culture supernatants were diluted in PBS-BSA 1% by serial dilution starting at 1:40 for serum and undiluted for supernatants. Standard curves of polyclonal IgM or IgG were obtained by serial dilution threefold for IgM and fivefold for IgG, starting at 1  $\mu$ g/ml for supernatants and 2  $\mu$ g/ml for serum samples. Secondary antibodies conjugated to HRP (Southern Biotech) were diluted

1:2,000 for IgM and 1:8,000 for IgG in PBS-BSA 1%. After wash with PBS, reactions were developed with TMB substrate solution (Sigma-Aldrich). The reaction was stopped with HCL 1N.

### ELISA for antigen-specific Ig detection

ELISAs to determine serum levels of anti-VLPs, anti-EDIII, anti-NS1, and anti-OVA antibodies, as well as specificity of IgG in B cell culture supernatants, were performed as previously described (Lucas et al., 2018). Briefly, 96-well plates (Costar) were coated with peptide (EDIII; 10  $\mu$ g/ml) or protein (1  $\mu$ g/ml) diluted in PBS and incubated at 4°C for 18 h. Serum samples were diluted following serial dilution 1:3 for IgM and IgG starting with 1:40 in the first well. ZIKV and DENV EDIII recombinant proteins were kindly provided by Dr. Orlando Ferreira, Institute of Biology, Universidade Federal do Rio de Janeiro, Rio de Janeiro, Brazil. VLPs were produced and purified as previously described (Alvim et al., 2019). ZIKV and DENV NS1 proteins were produced and purified as reported previously (Conde et al., 2016).

### Immunoblot

BALB/c tissues (brain and skeletal muscle) were dissociated by Polytron homogenizer (4,000 rpm) in homogenizing buffer (Tris-HCl 0.5 M, pH 6.8, SDS 10%, and Mili-Q water) as described by Haury et al. (1994). Tissue extracts were fractionated by electrophoresis in 10% polyacrylamide gel under denaturing conditions at 50 mA until 6 cm of migration. Proteins were transferred from the gel to a nitrocellulose membrane by a semi-dry electrotransfer (Semi-Dry Electrobloetter B) for 60 min at 0.8 mA/cm<sup>2</sup>. After transfer, the membrane was kept in 50 ml PBS/Tween 20 (Bio-Rad) at 0.2% vol/vol shaking for 18 h at room temperature.

Incubation of the membrane with cell culture supernatants or serum samples was performed in a Miniblot System Cassette (Immunetics), which allows the simultaneous incubation of 28 different samples in separated channels. Supernatants were diluted 1:2, and serum samples were diluted 1:100. After wash, membranes were incubated with secondary antibodies conjugated to alkaline phosphatase anti-IgM or anti-IgG diluted 1:2,000 (rabbit anti-mouse IgM; Jackson ImmunoResearch; goat anti-mouse IgG; Southern Biotech). Substrate NBT/BCIP (Promega) was added after wash. Reaction was developed shaking at room temperature and stopped with Milli-Q water. Colloidal gold staining was performed after scanning membranes.

### Flow cytometry and cell sorting

Cells were harvested from spleen and popliteal LNs for flow cytometry and cell sorting. Splenocytes were homogenized with complete RPMI 1640 medium (Gibco), followed by red blood cell lysis in 1 ml of ACK lysing buffer (Gibco) for 1 min on ice. Popliteal LNs were homogenized with complete RPMI 1640 medium (Gibco). Cells were washed and resuspended in an appropriate volume for counting and staining. Cells were stained with the following monoclonal antibodies conjugated to fluorochromes: anti-B220, CD38, CD138, GL-7, CD21, and CD23 (eBioscience) for 30 min at 4°C in FACS staining buffer (PBS 1 $\times$  with 5% FCS). Analysis and cell sort were then performed on a MoFlo (Dako-Cytomation) or Aria II (BD Biosciences). B cell

populations were defined as GC (B220<sup>+</sup> CD138<sup>-</sup> CD38<sup>lo/-</sup> GL-7<sup>+</sup>) and FO (B220<sup>+</sup> CD138<sup>-</sup> CD21<sup>lo/-</sup> CD23<sup>+</sup> GL-7<sup>-</sup>). Cells were collected directly in sterile tubes containing supplemented OptiMEM (Gibco) for cell culture.

### GC B cell culture in limiting dilution assay

Decreasing number of GC B cells were cultured in 250  $\mu$ l of OptiMEM (Gibco) supplemented with 10% heat-inactivated FBS (Gibco), 2 mM L-glutamine, 1 mM sodium pyruvate, 50  $\mu$ M 2-mercaptoethanol, 100 U penicillin, and 100  $\mu$ g/ml streptomycin. All cultures were performed in 96-well flat-bottom plates containing 3  $\times$  10<sup>3</sup> NB21 feeder cells/well as previously described with minor modifications (Kuraoka et al., 2016), mainly irradiating the feeder cells (20 Gy) and not adding IL-4. GC B cells were added starting from 3,000 cells/well to 1 cell/well through threefold dilution steps in the presence of 30  $\mu$ g/ml LPS (*Salmonella typhimurium*; Sigma-Aldrich). After 7 d, cultures were screened by ELISA to determine the frequency of IgG-secreting GC B cells according to the Poisson distribution (Andersson et al., 1977; Taswell, 1981).

### Single GC B cell cultures

Single GC B cells were cultured in OptiMEM (Gibco) supplemented with 10% heat-inactivated FBS (Gibco), 2 mM L-glutamine, 1 mM sodium pyruvate, 50  $\mu$ M 2-mercaptoethanol, 100 U penicillin, and 100  $\mu$ g/ml streptomycin. Cells were sorted into 96-well round-bottom plates containing 10<sup>3</sup> gamma-irradiated (20 Gy) NB21 cells/well, as previously described with minor modifications, mostly not adding IL-4 (Kuraoka et al., 2016). Supernatants were collected after 7 d of culture and cells were frozen in TCL lysis buffer supplemented with 1% 2-mercaptoethanol for *Igh* sequencing.

### *Igh* sequencing

Single GC B cells from popliteal LNs of BALB/c mice immunized with ZIKV or DENV NS1 proteins were sorted into 96-well PCR plates directly or after 7 d in culture. Plates contained 5  $\mu$ l TCL lysis buffer (Qiagen) supplemented with 1% 2-mercaptoethanol. RNA extraction was performed using Solid Phase Reversible Immobilization beads as described previously (Tas et al., 2016). RNA was reverse transcribed into cDNA using an oligo (dT) primer. *Igh* transcripts were amplified as described in (Tiller et al., 2009). PCR products were barcoded and sequenced using MiSeq (Illumina) Nano kit v.2 as described previously (Mesin et al., 2020).

Paired-end sequences were assembled with PandaSeq (Masella et al., 2012) and processed with the FASTX toolkit. The resulting demultiplexed and collapsed reads were assigned to wells according to barcodes. High-count sequences for every single cell/well were analyzed. Ig heavy chains were aligned to both IMGT (Lefranc et al., 2009) and Vbase2 (Retter et al., 2005) databases, and in case of discrepancy, IgBLAST was used. V<sub>H</sub> mutation analyses were restricted to cells with productively rearranged *Igh* genes, as described previously (Mesin et al., 2020). CDR-H3 analyses were performed as described previously (Ivanov et al., 2005). Average hydrophobicity of CDR-H3 was calculated as previously described (Kyte and

Doolittle, 1982). Functional rearrangements were grouped by clonotypes defined by the same  $V_H$  and  $J_H$  segment and identical CDR-H3 length and amino acid sequence. *Igh* sequencing data are available in Table S2.

### Statistical analyses

Statistical analyses were performed using GraphPad Prism 7.0 software. Tests were chosen according to the type of variable and indicated in each result. Results with  $P > 0.05$  were considered significant. Principal-component analysis was performed to compare the repertoires globally. Reactivity sections were defined, and signal intensities across the sections were quantified and analyzed as described previously (Mouthon et al., 1995).

### Online supplemental material

Fig. S1 shows the characterization of humoral immune response to UV-*i*ZIKV against ZIKV VLPs, ZIKV EDIII, and ZIKV NS1. Fig. S2 shows cross-reactivity with DENV EDIII and NS1 antigens, as well as the unrelated antigens heat shock protein Hsp60 and bacterial DNAK from *Escherichia coli*. Fig. S3 shows quantification of the number of responding GC B cell clones per culture secreting each BALB/c IgG subclass (IgG1, IgG2a, IgG2b, and IgG3). Fig. S4 shows the analysis of  $V_H$  family usage and CDR-H3 length of *Igh* transcripts from B cells present in GCs after ZIKV NS1 or DENV NS1 immunization. Fig. S5 shows antigen specificity of B cells in GCs after immunization with OVA against the immunizing antigen and self-antigens using brain extract immunoblots. Table S1 lists CDR-H3 characteristics from GC B cell clones tested for self-reactivity shown in Fig. 6. Table S2 is a summary of sequencing reads and reconstructed *Igh* VDJ sequences from ZNS1- and DNS1-immunized mice.

### Acknowledgments

We thank Dr. Orlando Ferreira for kindly providing ZIKV and DENV EDIII recombinant proteins; Dr. Edgar F.O. de Jesus (in memoriam) and his laboratory members for cell irradiation, and Dr. Garnett Kelsoe (Duke University, Durham, NC) for kindly providing the NB21 feeder cells. We thank Dr. Marcelo Bozza for helpful discussion and suggestions. We thank Phillippe Caloba and all members of the Laboratory of Lymphocyte Biology for assistance with experiments.

This work was supported by the Brazilian research funding agencies Fundação de Amparo à Pesquisa do Estado do Rio de Janeiro, Conselho Nacional de Desenvolvimento Científico e Tecnológico, Coordenação de Aperfeiçoamento de Pessoal de Nível Superior, and Financiadora de Estudos e Projetos. C.B. Cavazzoni was supported by Conselho Nacional de Desenvolvimento Científico e Tecnológico (PhD fellowship) and Coordenação de Aperfeiçoamento de Pessoal de Nível Superior (PDSE 88881.132337/2016-01 and Projeto de pesquisa 1759/2014, Bio-computacional, process no. 23038.004628/2014-66). G.D. Victora is a Burroughs Wellcome Fund Investigator in the Pathogenesis of Infectious Disease.

Author contributions: C.B. Cavazzoni and A.M. Vale conceptualized the study and designed the experiments. C.B.

Cavazzoni, V.B.T. Bozza, L. Tostes, L. Conde, B. Maia, J. Ersching, L. Mesin, A. Schiepers, H.A. de Paula Neto, and A.M. Vale performed experiments. L. Mesin, A. Schiepers, and H.A. de Paula Neto contributed to experiment design and analyzed data. J.N. Conde, D.R. Coelho, T.M. Lima, R.G.F. Alvim, L.R. Castilho, R. Mohana-Borges, and I. Assunção-Miranda generated resources. C.B. Cavazzoni and A.M. Vale analyzed the data and wrote the manuscript. A. Nobrega and G.D. Victora contributed to study design, data analyses, and manuscript writing.

Disclosures: The authors declare no competing financial interests.

Submitted: 12 March 2021

Revised: 24 May 2021

Accepted: 30 June 2021

### References

- Akey, D.L., W.C. Brown, S. Dutta, J. Konwerski, J. Jose, T.J. Jurkiw, J. Del-Proposto, C.M. Ogata, G. Skiniotis, R.J. Kuhn, and J.L. Smith. 2014. Flavivirus NS1 structures reveal surfaces for associations with membranes and the immune system. *Science*. 343:881–885. <https://doi.org/10.1126/science.1247749>
- Akkaya, M., B. Akkaya, A.S. Kim, P. Miozzo, H. Sohn, M. Pena, A.S. Roesler, B.P. Theall, T. Henke, J. Kabat, et al. 2018. Toll-like receptor 9 antagonizes antibody affinity maturation. *Nat. Immunol.* 19:255–266. <https://doi.org/10.1038/s41590-018-0052-z>
- Alvim, R.G.F., I. Itabaiana Jr., and L.R. Castilho. 2019. Zika virus-like particles (VLPs): Stable cell lines and continuous perfusion processes as a new potential vaccine manufacturing platform. *Vaccine*. 37:6970–6977. <https://doi.org/10.1016/j.vaccine.2019.05.064>
- Andersson, J., A. Coutinho, W. Lernhardt, and F. Melchers. 1977. Clonal growth and maturation to immunoglobulin secretion in vitro of every growth-inducible B lymphocyte. *Cell*. 10:27–34. [https://doi.org/10.1016/0092-8674\(77\)90136-2](https://doi.org/10.1016/0092-8674(77)90136-2)
- Andreano, E., and R. Rappuoli. 2021. Immunodominant antibody germlines in COVID-19. *J. Exp. Med.* 218:e20210281. <https://doi.org/10.1084/jem.20210281>
- Andreano, E., E. Nicastrì, I. Paciello, P. Pileri, N. Manganaro, G. Piccini, A. Manenti, E. Pantano, A. Kabanova, M. Troisi, et al. 2021. Extremely potent human monoclonal antibodies from COVID-19 convalescent patients. *Cell*. 184:1821–1835.e16. <https://doi.org/10.1016/j.cell.2021.02.035>
- Avirutnan, P., A. Fuchs, R.E. Hahart, P. Somnuk, S. Youn, M.S. Diamond, and J.P. Atkinson. 2010. Antagonism of the complement component C4 by flavivirus nonstructural protein NS1. *J. Exp. Med.* 207:793–806. <https://doi.org/10.1084/jem.20092545>
- Bailey, M.J., F. Broecker, J. Duehr, F. Arumemi, F. Krammer, P. Palese, and G.S. Tan. 2019. Antibodies Elicited by an NS1-Based Vaccine Protect Mice against Zika Virus. *MBio*. 10:e02861-18. <https://doi.org/10.1128/mBio.02861-18>
- Balakrishnan, T., D.B. Bela-Ong, Y.X. Toh, M. Flamand, S. Devi, M.B. Koh, M.L. Hibberd, E.E. Ooi, J.G. Low, Y.S. Leo, et al. 2011. Dengue virus activates polyreactive, natural IgG B cells after primary and secondary infection. *PLoS One*. 6:e29430. <https://doi.org/10.1371/journal.pone.0029430>
- Barbi, L., A.V.C. Coelho, L.C.A. Alencar, and S. Crovella. 2018. Prevalence of Guillain-Barré syndrome among Zika virus infected cases: a systematic review and meta-analysis. *Braz. J. Infect. Dis.* 22:137–141. <https://doi.org/10.1016/j.bjid.2018.02.005>
- Bardina, S.V., P. Bunduc, S. Tripathi, J. Duehr, J.J. Frere, J.A. Brown, R. Nachbagauer, G.A. Foster, D. Krysztof, D. Tortorella, et al. 2017. Enhancement of Zika virus pathogenesis by preexisting ant flavivirus immunity. *Science*. 356:175–180. <https://doi.org/10.1126/science.aal4365>
- Bastard, P., L.B. Rosen, Q. Zhang, E. Michailidis, H.H. Hoffmann, Y. Zhang, K. Dorgham, Q. Philippot, J. Rosain, V. Béziat, et al. COVID Human Genetic Effort. 2020. Autoantibodies against type I IFNs in patients with life-threatening COVID-19. *Science*. 370:eabd4585. <https://doi.org/10.1126/science.abd4585>

- Beasley, D.W., and A.D. Barrett. 2002. Identification of neutralizing epitopes within structural domain III of the West Nile virus envelope protein. *J. Virol.* 76:13097–13100. <https://doi.org/10.1128/JVI.76.24.13097-13100.2002>
- Beatty, P.R., H. Puerta-Guardo, S.S. Killingbeck, D.R. Glasner, K. Hopkins, and E. Harris. 2015. Dengue virus NS1 triggers endothelial permeability and vascular leak that is prevented by NS1 vaccination. *Sci. Transl. Med.* 7: 304ra141. <https://doi.org/10.1126/scitranslmed.aaa3787>
- Bessa, J., M. Kopf, and M.F. Bachmann. 2010. Cutting edge: IL-21 and TLR signaling regulate germinal center responses in a B cell-intrinsic manner. *J. Immunol.* 184:4615–4619. <https://doi.org/10.4049/jimmunol.0903949>
- Biering, S.B., D.L. Akey, M.P. Wong, W.C. Brown, N.T.N. Lo, H. Puerta-Guardo, F. Tramontini Gomes de Sousa, C. Wang, J.R. Konwerski, D.A. Espinosa, et al. 2021. Structural basis for antibody inhibition of flavivirus NS1-triggered endothelial dysfunction. *Science.* 371:194–200. <https://doi.org/10.1126/science.abc0476>
- Brown, W.C., D.L. Akey, J.R. Konwerski, J.T. Tarrasch, G. Skiniotis, R.J. Kuhn, and J.L. Smith. 2016. Extended surface for membrane association in Zika virus NS1 structure. *Nat. Struct. Mol. Biol.* 23:865–867. <https://doi.org/10.1038/nsmb.3268>
- Burnett, D.L., D.B. Langley, P. Schofield, J.R. Hermes, T.D. Chan, J. Jackson, K. Bourne, J.H. Reed, K. Patterson, B.T. Porebski, et al. 2018. Germinal center antibody mutation trajectories are determined by rapid self/foreign discrimination. *Science.* 360:223–226. <https://doi.org/10.1126/science.aao3859>
- Cheng, H.J., C.F. Lin, H.Y. Lei, H.S. Liu, T.M. Yeh, Y.H. Luo, and Y.S. Lin. 2009. Proteomic analysis of endothelial cell autoantigens recognized by anti-dengue virus nonstructural protein 1 antibodies. *Exp. Biol. Med. (Maywood).* 234:63–73. <https://doi.org/10.3181/0805-RM-147>
- Chuang, Y.C., J. Lin, Y.S. Lin, S. Wang, and T.M. Yeh. 2016. Dengue Virus Nonstructural Protein 1-Induced Antibodies Cross-React with Human Plasminogen and Enhance Its Activation. *J. Immunol.* 196:1218–1226. <https://doi.org/10.4049/jimmunol.1500057>
- Coelho, S.V.A., R.L.S. Neris, M.P. Papa, L.C. Schnellrath, L.M. Meuren, D.A. Tschoeke, L. Leomil, B.R.F. Verçoza, M. Miranda, F.L. Thompson, et al. 2017. Development of standard methods for Zika virus propagation, titration, and purification. *J. Virol. Methods.* 246:65–74. <https://doi.org/10.1016/j.jviromet.2017.04.011>
- Conde, J.N., E.M. da Silva, D. Allonso, D.R. Coelho, I.D.S. Andrade, L.N. de Medeiros, J.L. Menezes, A.S. Barbosa, and R. Mohana-Borges. 2016. Inhibition of the Membrane Attack Complex by Dengue Virus NS1 through Interaction with Vitronectin and Terminal Complement Proteins. *J. Virol.* 90:9570–9581. <https://doi.org/10.1128/JVI.00912-16>
- Coutelier, J.P., J.T. van der Logt, F.W. Heessen, G. Warnier, and J. Van Snick. 1987. IgG2a restriction of murine antibodies elicited by viral infections. *J. Exp. Med.* 165:64–69. <https://doi.org/10.1084/jem.165.1.64>
- Cox, B.D., R.A. Stanton, and R.F. Schinazi. 2015. Predicting Zika virus structural biology: Challenges and opportunities for intervention. *Antivir. Chem. Chemother.* 24:118–126. <https://doi.org/10.1177/2040206616653873>
- Csurhes, P.A., A.A. Sullivan, K. Green, M.P. Pender, and P.A. McCombe. 2005. T cell reactivity to PO, P2, PMP-22, and myelin basic protein in patients with Guillain-Barre syndrome and chronic inflammatory demyelinating polyradiculoneuropathy. *J. Neurol. Neurosurg. Psychiatry.* 76: 1431–1439. <https://doi.org/10.1136/jnnp.2004.052282>
- Dai, L., J. Song, X. Lu, Y.Q. Deng, A.M. Musyoki, H. Cheng, Y. Zhang, Y. Yuan, H. Song, J. Haywood, et al. 2016. Structures of the Zika Virus Envelope Protein and Its Complex with a Flavivirus Broadly Protective Antibody. *Cell Host Microbe.* 19:696–704. <https://doi.org/10.1016/j.chom.2016.04.013>
- Das, A., B.A. Heesters, A. Bialas, J. O'Flynn, I.R. Rifkin, J. Ochando, N. Mittereder, G. Carlesso, R. Herbst, and M.C. Carroll. 2017. Follicular Dendritic Cell Activation by TLR Ligands Promotes Autoreactive B Cell Responses. *Immunity.* 46:106–119. <https://doi.org/10.1016/j.immuni.2016.12.014>
- de Oliveira, W.K., G.V.A. de França, E.H. Carmo, B.B. Duncan, R. de Souza Kuchenbecker, and M.I. Schmidt. 2017. Infection-related microcephaly after the 2015 and 2016 Zika virus outbreaks in Brazil: a surveillance-based analysis. *Lancet.* 390:861–870. [https://doi.org/10.1016/S0140-6736\(17\)31368-5](https://doi.org/10.1016/S0140-6736(17)31368-5)
- Degn, S.E., C.E. van der Poel, D.J. Firl, B. Ayoglu, F.A. Al Qureshah, G. Bajic, L. Mesin, C.A. Reynaud, J.C. Weill, P.J. Utz, et al. 2017. Clonal Evolution of Autoreactive Germinal Centers. *Cell.* 170:913–926.e19. <https://doi.org/10.1016/j.cell.2017.07.026>
- Demengeot, J., R. Vasconcellos, Y. Modigliani, A. Grandien, and A. Coutinho. 1997. B lymphocyte sensitivity to IgM receptor ligation is independent of maturation stage and locally determined by macrophage-derived IFN-beta. *Int. Immunol.* 9:1677–1685. <https://doi.org/10.1093/intimm/9.11.1677>
- Dowall, S.D., V.A. Graham, E. Rayner, B. Atkinson, G. Hall, R.J. Watson, A. Bosworth, L.C. Bonney, S. Kitchen, and R. Hewson. 2016. A Susceptible Mouse Model for Zika Virus Infection. *PLoS Negl. Trop. Dis.* 10: e0004658. <https://doi.org/10.1371/journal.pntd.0004658>
- Elong Ngonu, A., M.P. Young, M. Bunz, Z. Xu, S. Hattakam, E. Vizcarra, J.A. Regla-Nava, W.W. Tang, M. Yamabhai, J. Wen, and S. Shresta. 2019. CD4+ T cells promote humoral immunity and viral control during Zika virus infection. *PLoS Pathog.* 15:e1007474. <https://doi.org/10.1371/journal.ppat.1007474>
- Falconar, A.K. 1997. The dengue virus nonstructural-1 protein (NS1) generates antibodies to common epitopes on human blood clotting, integrin/adhesin proteins and binds to human endothelial cells: potential implications in haemorrhagic fever pathogenesis. *Arch. Virol.* 142: 897–916. <https://doi.org/10.1007/s007050050127>
- Fallet, B., K. Narr, Y.I. Ertuna, M. Remy, R. Sommerstein, K. Cornille, M. Kreutzfeldt, N. Page, G. Zimmer, F. Geier, et al. 2016. Interferon-driven deletion of antiviral B cells at the onset of chronic infection. *Sci. Immunol.* 1:eaa6817.
- Freire, M.C.L.C., L. Pol-Fachin, D.F. Coêlho, I.F.T. Viana, T. Magalhães, M.T. Cordeiro, N. Fischer, F.F. Loeffler, T. Jaenisch, R.F. Franca, et al. 2017. Mapping Putative B-Cell Zika Virus NS1 Epitopes Provides Molecular Basis for Anti-NS1 Antibody Discrimination between Zika and Dengue Viruses. *ACS Omega.* 2:3913–3920. <https://doi.org/10.1021/acsomega.7b00608>
- Füst, G., Z. Beck, D. Bánhegyi, J. Kocsis, A. Bíró, and Z. Prohászka. 2005. Antibodies against heat shock proteins and cholesterol in HIV infection. *Mol. Immunol.* 42:79–85. <https://doi.org/10.1016/j.molimm.2004.07.003>
- Gao, X., Y. Wen, J. Wang, W. Hong, C. Li, L. Zhao, C. Yin, X. Jin, F. Zhang, and L. Yu. 2018. Delayed and highly specific antibody response to non-structural protein 1 (NS1) revealed during natural human ZIKV infection by NS1-based capture ELISA. *BMC Infect. Dis.* 18:275. <https://doi.org/10.1186/s12879-018-3173-y>
- Gonçalves, A.J., E.R. Oliveira, S.M. Costa, M.V. Paes, J.F. Silva, A.S. Azevedo, M. Mantuano-Barradas, A.C. Nogueira, C.J. Almeida, and A.M. Alves. 2015. Cooperation between CD4+ T Cells and Humoral Immunity Is Critical for Protection against Dengue Using a DNA Vaccine Based on the NS1 Antigen. *PLoS Negl. Trop. Dis.* 9:e0004277. <https://doi.org/10.1371/journal.pntd.0004277>
- Hassert, M., K.J. Wolf, K.E. Schwetye, R.J. DiPaolo, J.D. Brien, and A.K. Pinto. 2018. CD4+T cells mediate protection against Zika associated severe disease in a mouse model of infection. *PLoS Pathog.* 14:e1007237. <https://doi.org/10.1371/journal.ppat.1007237>
- Haurly, M., A. Grandien, A. Sundblad, A. Coutinho, and A. Nobrega. 1994. Global analysis of antibody repertoires. I. An immunoblot method for the quantitative screening of a large number of reactivities. *Scand. J. Immunol.* 39:79–87. <https://doi.org/10.1111/j.1365-3083.1994.tb03343.x>
- Heesters, B.A., R.C. Myers, and M.C. Carroll. 2014. Follicular dendritic cells: dynamic antigen libraries. *Nat. Rev. Immunol.* 14:495–504. <https://doi.org/10.1038/nri3689>
- Hilgenfeld, R. 2016. Zika virus NS1, a pathogenicity factor with many faces. *EMBO J.* 35:2631–2633. <https://doi.org/10.15252/embj.201695871>
- Huang, H., S. Li, Y. Zhang, X. Han, B. Jia, H. Liu, D. Liu, S. Tan, Q. Wang, Y. Bi, et al. 2017. CD8+ T Cell Immune Response in Immunocompetent Mice during Zika Virus Infection. *J. Virol.* 91:e00900-17. <https://doi.org/10.1128/JVI.00900-17>
- Hunziker, L., M. Recher, A.J. Macpherson, A. Ciurea, S. Freigang, H. Hengartner, and R.M. Zinkernagel. 2003. Hypergammaglobulinemia and autoantibody induction mechanisms in viral infections. *Nat. Immunol.* 4:343–349. <https://doi.org/10.1038/ni911>
- Ivanov, I.I., R.L. Schelonka, Y. Zhuang, G.L. Gartland, M. Zemlin, and H.W. Schroeder Jr. 2005. Development of the expressed Ig CDR-H3 repertoire is marked by focusing of constraints in length, amino acid use, and charge that are first established in early B cell progenitors. *J. Immunol.* 174:7773–7780. <https://doi.org/10.4049/jimmunol.174.12.7773>
- Kiefer, K., M.A. Oropallo, M.P. Cancro, and A. Marshak-Rothstein. 2012. Role of type I interferons in the activation of autoreactive B cells. *Immunol. Cell Biol.* 90:498–504. <https://doi.org/10.1038/ich.2012.10>
- Kreer, C., M. Zehner, T. Weber, M.S. Ercanoglu, L. Gieselmann, C. Rohde, S. Halwe, M. Korenkov, P. Schommers, K. Vanshylla, et al. 2020. Longitudinal Isolation of Potent Near-Germline SARS-CoV-2-Neutralizing

- Antibodies from COVID-19 Patients. *Cell*. 182:843–854.e12. <https://doi.org/10.1016/j.cell.2020.06.044>
- Kuraoka, M., A.G. Schmidt, T. Nojima, F. Feng, A. Watanabe, D. Kitamura, S.C. Harrison, T.B. Kepler, and G. Kelsoe. 2016. Complex Antigens Drive Permissive Clonal Selection in Germinal Centers. *Immunity*. 44:542–552. <https://doi.org/10.1016/j.immuni.2016.02.010>
- Kyte, J., and R.F. Doolittle. 1982. A simple method for displaying the hydrophobic character of a protein. *J. Mol. Biol.* 157:105–132. [https://doi.org/10.1016/0022-2836\(82\)90515-0](https://doi.org/10.1016/0022-2836(82)90515-0)
- Lardone, R.D., N. Yuki, M. Odaka, J.L. Daniotti, F.J. Irazoqui, and G.A. Nores. 2010. Anti-GM1 IgG antibodies in Guillain-Barré syndrome: fine specificity is associated with disease severity. *J. Neurol. Neurosurg. Psychiatry*. 81:629–633. <https://doi.org/10.1136/jnnp.2009.183665>
- Lazar, H.M., J. Govero, A.M. Smith, D.J. Platt, E. Fernandez, J.J. Miner, and M.S. Diamond. 2016. A Mouse Model of Zika Virus Pathogenesis. *Cell Host Microbe*. 19:720–730. <https://doi.org/10.1016/j.chom.2016.03.010>
- Lee, P.X., D.H.R. Ting, C.P.H. Boey, E.T.X. Tan, J.Z.H. Chia, F. Idris, Y. Oo, L.C. Ong, Y.L. Chua, C. Hapuarachchi, et al. 2020. Relative contribution of nonstructural protein 1 in dengue pathogenesis. *J. Exp. Med.* 217:e20191548. <https://doi.org/10.1084/jem.20191548>
- Lefranc, M.P., V. Giudicelli, C. Ginestoux, J. Jabado-Michaloud, G. Folch, F. Bellahcene, Y. Wu, E. Gemrot, X. Brochet, J. Lane, et al. 2009. IMGT, the international ImMunoGeneTics information system. *Nucleic Acids Res.* 37(Database):D1006–D1012. <https://doi.org/10.1093/nar/gkn838>
- Lucas, C.G.O., J.Z. Kitoko, F.M. Ferreira, V.G. Suzart, M.P. Papa, S.V.A. Coelho, C.B. Cavazzoni, H.A. Paula-Neto, P.C. Olsen, A. Iwasaki, et al. 2018. Critical role of CD4<sup>+</sup> T cells and IFN $\gamma$  signaling in antibody-mediated resistance to Zika virus infection. *Nat. Commun.* 9:3136. <https://doi.org/10.1038/s41467-018-05519-4>
- Masella, A.P., A.K. Bartram, J.M. Truszkowski, D.G. Brown, and J.D. Neufeld. 2012. PANDAseq: paired-end assembler for illumina sequences. *BMC Bioinformatics*. 13:31. <https://doi.org/10.1186/1471-2105-13-31>
- Mesin, L., A. Schiepers, J. Ersching, A. Barbulescu, C.B. Cavazzoni, A. Angelini, T. Okada, T. Kurosaki, and G.D. Victora. 2020. Restricted Clonality and Limited Germinal Center Reentry Characterize Memory B Cell Reactivation by Boosting. *Cell*. 180:92–106.e11. <https://doi.org/10.1016/j.cell.2019.11.032>
- Modhiran, N., D. Watterson, D.A. Muller, A.K. Panetta, D.P. Sester, L. Liu, D.A. Hume, K.J. Stacey, and P.R. Young. 2015. Dengue virus NS1 protein activates cells via Toll-like receptor 4 and disrupts endothelial cell monolayer integrity. *Sci. Transl. Med.* 7:304ra142. <https://doi.org/10.1126/scitranslmed.aaa3863>
- Modhiran, N., H. Song, L. Liu, C. Bletchly, L. Brillault, A.A. Amarilla, X. Xu, J. Qi, Y. Chai, S.T.M. Cheung, et al. 2021. A broadly protective antibody that targets the flavivirus NS1 protein. *Science*. 371:190–194. <https://doi.org/10.1126/science.abb9425>
- Molnarfi, N., U. Schulze-Toppoff, M.S. Weber, J.C. Patarroyo, T. Prod'homme, M. Varrin-Doyer, A. Shetty, C. Linington, A.J. Slavina, J. Hidalgo, et al. 2013. MHC class II-dependent B cell APC function is required for induction of CNS autoimmunity independent of myelin-specific antibodies. *J. Exp. Med.* 210:2921–2937. <https://doi.org/10.1084/jem.20130699>
- Mouthon, L., A. Nobrega, N. Nicolas, S.V. Kaveri, C. Barreau, A. Coutinho, and M.D. Kazatchkine. 1995. Invariance and restriction toward a limited set of self-antigens characterize neonatal IgM antibody repertoires and prevail in autoreactive repertoires of healthy adults. *Proc. Natl. Acad. Sci. USA*. 92:3839–3843. <https://doi.org/10.1073/pnas.92.9.3839>
- Muller, D.A., and P.R. Young. 2013. The flavivirus NS1 protein: molecular and structural biology, immunology, role in pathogenesis and application as a diagnostic biomarker. *Antiviral Res.* 98:192–208. <https://doi.org/10.1016/j.antiviral.2013.03.008>
- Nobrega, A., M. Haury, A. Grandien, E. Malanchère, A. Sundblad, and A. Coutinho. 1993. Global analysis of antibody repertoires. II. Evidence for specificity, self-selection and the immunological “homunculus” of antibodies in normal serum. *Eur. J. Immunol.* 23:2851–2859. <https://doi.org/10.1002/eji.1830231119>
- Nobrega, A., A. Grandien, M. Haury, L. Hecker, E. Malanchère, and A. Coutinho. 1998. Functional diversity and clonal frequencies of reactivity in the available antibody repertoire. *Eur. J. Immunol.* 28:1204–1215. [https://doi.org/10.1002/\(SICI\)1521-4141\(199804\)28:04<1204::AID-IMMU1204>3.0.CO;2-G](https://doi.org/10.1002/(SICI)1521-4141(199804)28:04<1204::AID-IMMU1204>3.0.CO;2-G)
- Oliphant, T., M. Engle, G.E. Nybakken, C. Doane, S. Johnson, L. Huang, S. Gorlatov, E. Mehlhop, A. Marri, K.M. Chung, et al. 2005. Development of a humanized monoclonal antibody with therapeutic potential against West Nile virus. *Nat. Med.* 11:522–530. <https://doi.org/10.1038/nm1240>
- Pardy, R.D., M.M. Rajah, S.A. Condotta, N.G. Taylor, S.M. Sagan, and M.J. Richer. 2017. Analysis of the T Cell Response to Zika Virus and Identification of a Novel CD8<sup>+</sup> T Cell Epitope in Immunocompetent Mice. *PLoS Pathog.* 13:e1006184. <https://doi.org/10.1371/journal.ppat.1006184>
- Puerta-Guardo, H., D.R. Glasner, D.A. Espinosa, S.B. Biering, M. Patana, K. Ratnasiri, C. Wang, P.R. Beatty, and E. Harris. 2019. Flavivirus NS1 Triggers Tissue-Specific Vascular Endothelial Dysfunction Reflecting Disease Tropism. *Cell Rep.* 26:1598–1613.e8. <https://doi.org/10.1016/j.celrep.2019.01.036>
- Quintana, F.J., and I.R. Cohen. 2011. The HSP60 immune system network. *Trends Immunol.* 32:89–95. <https://doi.org/10.1016/j.it.2010.11.001>
- Radic, M.Z., and M. Weigert. 1994. Genetic and structural evidence for antigen selection of anti-DNA antibodies. *Annu. Rev. Immunol.* 12:487–520. <https://doi.org/10.1146/annurev.iy.12.040194.002415>
- Radic, M.Z., and M. Weigert. 1995. Origins of anti-DNA antibodies and their implications for B-cell tolerance. *Ann. N. Y. Acad. Sci.* 764:384–396. <https://doi.org/10.1111/j.1749-6632.1995.tb55853.x>
- Radic, M.Z., J. Erikson, S. Litwin, and M. Weigert. 1993. B lymphocytes may escape tolerance by revising their antigen receptors. *J. Exp. Med.* 177:1165–1173. <https://doi.org/10.1084/jem.177.4.1165>
- Retter, I., H.H. Althaus, R. Münch, and W. Müller. 2005. VBASE2, an integrative V gene database. *Nucleic Acids Res.* 33:D671–D674. <https://doi.org/10.1093/nar/gki088>
- Reyes-Sandoval, A., and J.E. Ludert. 2019. The Dual Role of the Antibody Response Against the Flavivirus Non-structural Protein 1 (NS1) in Protection and Immuno-Pathogenesis. *Front. Immunol.* 10:1651. <https://doi.org/10.3389/fimmu.2019.01651>
- Richner, J.M., B.W. Jagger, C. Shan, C.R. Fontes, K.A. Dowd, B. Cao, S. Himansu, E.A. Caine, B.T.D. Nunes, D.B.A. Medeiros, et al. 2017. Vaccine Mediated Protection Against Zika Virus-Induced Congenital Disease. *Cell*. 170:273–283.e12. <https://doi.org/10.1016/j.cell.2017.06.040>
- Root-Bernstein, R., and D. Fairweather. 2014. Complexities in the relationship between infection and autoimmunity. *Curr. Allergy Asthma Rep.* 14:407. <https://doi.org/10.1007/s11882-013-0407-3>
- Sekiguchi, D.R., L. Yunk, D. Gary, D. Charan, B. Srivastava, D. Allman, M.G. Weigert, and E.T. Prak. 2006. Development and selection of edited B cells in B6.56R mice. *J. Immunol.* 176:6879–6887. <https://doi.org/10.4049/jimmunol.176.11.6879>
- Shrestha, B., J.D. Brien, S. Sukupolvi-Petty, S.K. Austin, M.A. Edeling, T. Kim, K.M. O'Brien, C.A. Nelson, S. Johnson, D.H. Fremont, and M.S. Diamond. 2010. The development of therapeutic antibodies that neutralize homologous and heterologous genotypes of dengue virus type 1. *PLoS Pathog.* 6:e1000823. <https://doi.org/10.1371/journal.ppat.1000823>
- Silva-Sanchez, A., C.R. Liu, A.M. Vale, M. Khass, P. Kapoor, A. Elgavish, I.I. Ivanov, G.C. Ippolito, R.L. Schelonka, T.R. Schoeb, et al. 2015. Violation of an evolutionarily conserved immunoglobulin diversity gene sequence preference promotes production of dsDNA-specific IgG antibodies. *PLoS One*. 10:e0118171. <https://doi.org/10.1371/journal.pone.0118171>
- Stettler, K., M. Beltramello, D.A. Espinosa, V. Graham, A. Cassotta, S. Bianchi, F. Vanzetta, A. Minola, S. Jaconi, F. Mele, et al. 2016. Specificity, cross-reactivity, and function of antibodies elicited by Zika virus infection. *Science*. 353:823–826. <https://doi.org/10.1126/science.aaf8505>
- Tas, J.M., L. Mesin, G. Pasqual, S. Targ, J.T. Jacobsen, Y.M. Mano, C.S. Chen, J.C. Weill, C.A. Reynaud, E.P. Browne, et al. 2016. Visualizing antibody affinity maturation in germinal centers. *Science*. 351:1048–1054. <https://doi.org/10.1126/science.aad3439>
- Taswell, C. 1981. Limiting dilution assays for the determination of immunocompetent cell frequencies. I. Data analysis. *J. Immunol.* 126:1614–1619.
- Tiller, T., C.E. Busse, and H. Wardemann. 2009. Cloning and expression of murine Ig genes from single B cells. *J. Immunol. Methods*. 350:183–193. <https://doi.org/10.1016/j.jim.2009.08.009>
- Vale, A.M., E. Hayashi, A. Granato, H.W. Schroeder Jr., M. Bellio, and A. Nobrega. 2010. Genetic control of the B cell response to LPS: opposing effects in peritoneal versus splenic B cell populations. *Immunogenetics*. 62:41–48. <https://doi.org/10.1007/s00251-009-0404-9>
- Vale, A.M., J.B. Foote, A. Granato, Y. Zhuang, R.M. Pereira, U.G. Lopes, M. Bellio, P.D. Burrows, H.W. Schroeder Jr., and A. Nobrega. 2012. A rapid and quantitative method for the evaluation of V gene usage, specificities and the clonal size of B cell repertoires. *J. Immunol. Methods*. 376:143–149. <https://doi.org/10.1016/j.jim.2011.12.005>
- Viant, C., G.H.J. Weymar, A. Escolano, S. Chen, H. Hartweg, M. Cipolla, A. Gazumyan, and M.C. Nussenzweig. 2020. Antibody Affinity Shapes the Choice between Memory and Germinal Center B Cell Fates. *Cell*. 183:1298–1311.e11. <https://doi.org/10.1016/j.cell.2020.09.063>
- Victora, G.D., and M.C. Nussenzweig. 2012. Germinal centers. *Annu. Rev. Immunol.* 30:429–457. <https://doi.org/10.1146/annurev-immunol-020711-075032>

- Victora, G.D., A.M. Bilate, A. Socorro-Silva, C. Caldas, R.C. Lima, J. Kalil, V. Coelho, and C.G. Victora. 2007. Mother-child immunological interactions in early life affect long-term humoral autoreactivity to heat shock protein 60 at age 18 years. *J. Autoimmun.* 29:38–43. <https://doi.org/10.1016/j.jaut.2007.02.018>
- Wang, J., M. Bardelli, D.A. Espinosa, M. Pedotti, T.S. Ng, S. Bianchi, L. Simonelli, E.X.Y. Lim, M. Foglierini, F. Zatta, et al. 2017. A Human B-specific Antibody against Zika Virus with High Therapeutic Potential. *Cell.* 171:229–241.e15. <https://doi.org/10.1016/j.cell.2017.09.002>
- Wardemann, H., S. Yurasov, A. Schaefer, J.W. Young, E. Meffre, and M.C. Nussenzweig. 2003. Predominant autoantibody production by early human B cell precursors. *Science.* 301:1374–1377. <https://doi.org/10.1126/science.1086907>
- Watterson, D., N. Modhiran, and P.R. Young. 2016. The many faces of the flavivirus NS1 protein offer a multitude of options for inhibitor design. *Antiviral Res.* 130:7–18. <https://doi.org/10.1016/j.antiviral.2016.02.014>
- Winkler, C.W., L.M. Myers, T.A. Woods, R.J. Messer, A.B. Carmody, K.L. McNally, D.P. Scott, K.J. Hasenkrug, S.M. Best, and K.E. Peterson. 2017. Adaptive Immune Responses to Zika Virus Are Important for Controlling Virus Infection and Preventing Infection in Brain and Testes. *J. Immunol.* 198:3526–3535. <https://doi.org/10.4049/jimmunol.1601949>
- Yauch, L.E., and S. Shresta. 2008. Mouse models of dengue virus infection and disease. *Antiviral Res.* 80:87–93. <https://doi.org/10.1016/j.antiviral.2008.06.010>
- Young, P.R., P.A. Hilditch, C. Bletchly, and W. Halloran. 2000. An antigen capture enzyme-linked immunosorbent assay reveals high levels of the dengue virus protein NS1 in the sera of infected patients. *J. Clin. Microbiol.* 38:1053–1057. <https://doi.org/10.1128/JCM.38.3.1053-1057.2000>
- Zellweger, R.M., T.R. Prestwood, and S. Shresta. 2010. Enhanced infection of liver sinusoidal endothelial cells in a mouse model of antibody-induced severe dengue disease. *Cell Host Microbe.* 7:128–139. <https://doi.org/10.1016/j.chom.2010.01.004>

Supplemental material

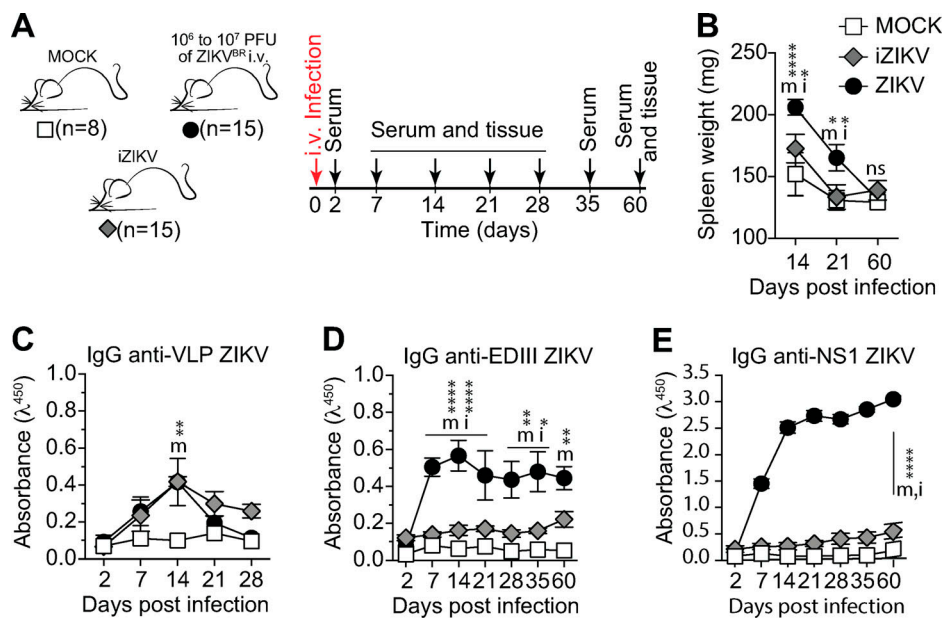


Figure S1. **Characterization of humoral immune response to UV-iZIKV.** (A) Experimental design indicating the time points of serum samples and lymphoid tissue collections from control mice (MOCK), mice immunized with UV-inactivated virus (iZIKV), and infected mice (ZIKV). (B) Spleen weight measured at the time of collection, as indicated. (C-E) Serum levels of IgG specific to VLP (C), domain III of ZIKV envelope protein (D), and NS1 (E). Measured by ELISA at 1:120 dilution. One experiment was performed with the indicated number of mice per group. Statistical analyses were performed using the unpaired two-tailed Student's *t* test. Significantly different from mock: m\*,  $P \leq 0.05$ ; m\*\*,  $P \leq 0.01$ ; m\*\*\*\*,  $P \leq 0.0001$ . Significantly different from iZIKV: i\*,  $P \leq 0.05$ ; i\*\*\*\*,  $P \leq 0.0001$ . Error bars represent SEM.

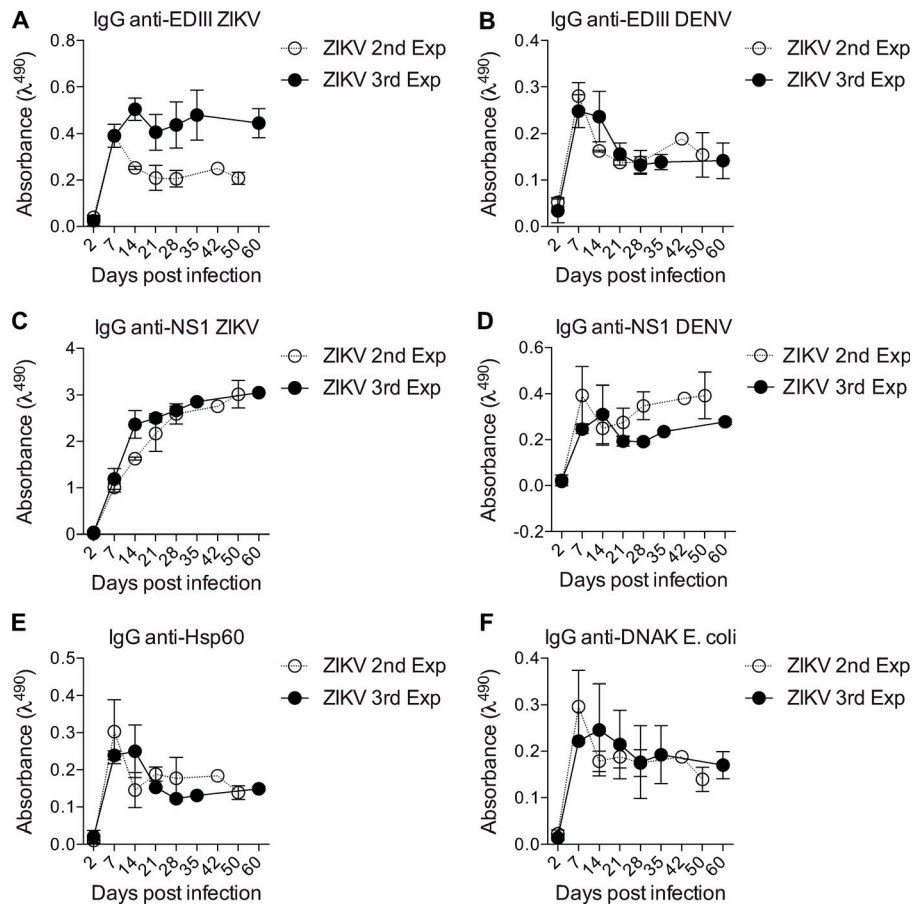


Figure S2. **Cross-reactivity with unrelated antigens. (A-F)** Sera from ZIKV-infected mice (1:120 dilution) from two independent experiments were tested by ELISA for binding to ZIKV and DENV antigens EDIII (A and B) and NS1 (C and D) as well as unrelated antigens heat shock protein (E and F) Hsp60 and bacterial DNAK from *E. coli* at different time points. The second experiment ended at 50 d and the third experiment at 60 d. Error bars represent SEM.

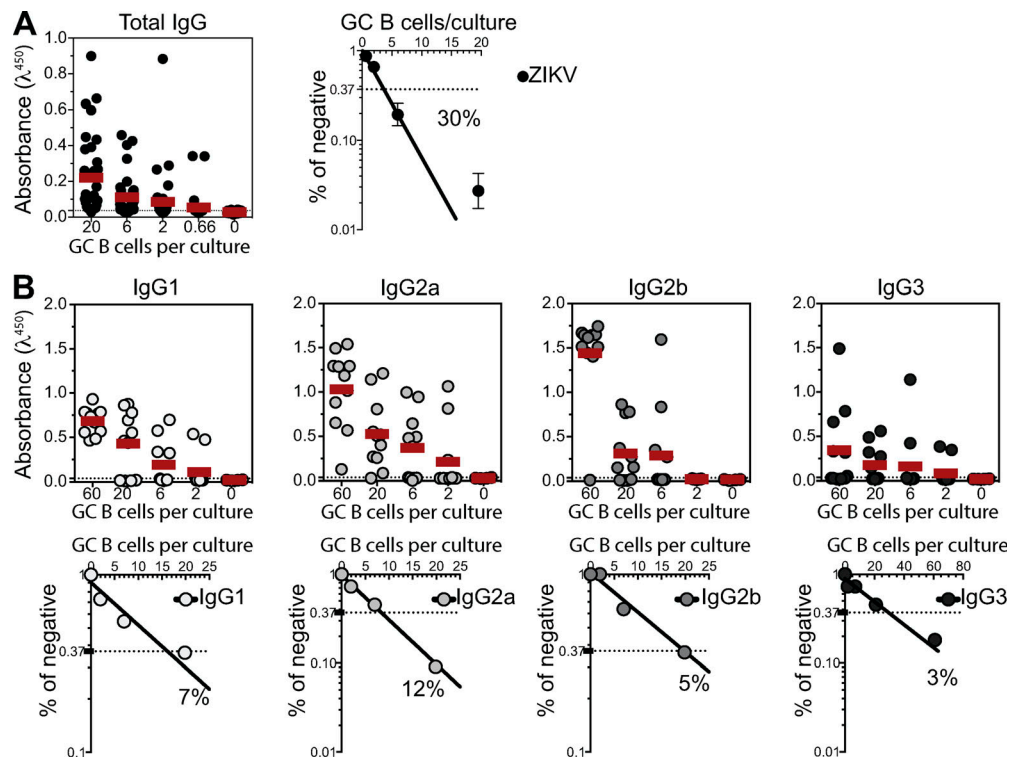


Figure S3. **Quantification of the number of responding GC B cell clones per culture.** GC B cells from popliteal LNs of ZIKV-infected mice were sorted and cultured in decreasing average number of cells per well (60, 20, 6, 2, and 0.66 cells/well). Supernatants were collected on day 7 and screened for IgG secretion by ELISA. **(A)** Frequency of GC B cell clones secreting total IgG per culture in response to polyclonal stimuli were calculated using Poisson distribution. **(B)** Culture supernatants were used to estimate the frequency of GC B cell clones secreting each BALB/c IgG subclass (IgG1, IgG2a, IgG2b, and IgG3). Cell culture was performed on a monolayer of gamma-irradiated (20 Gy) NB21 feeder cells (Kuraoka et al., 2016;  $3 \times 10^3$  cells/well) and LPS (30  $\mu$ g/ml). Data from one experiment with three mice per group. GC B cells from all mice in each group were pooled in culture.

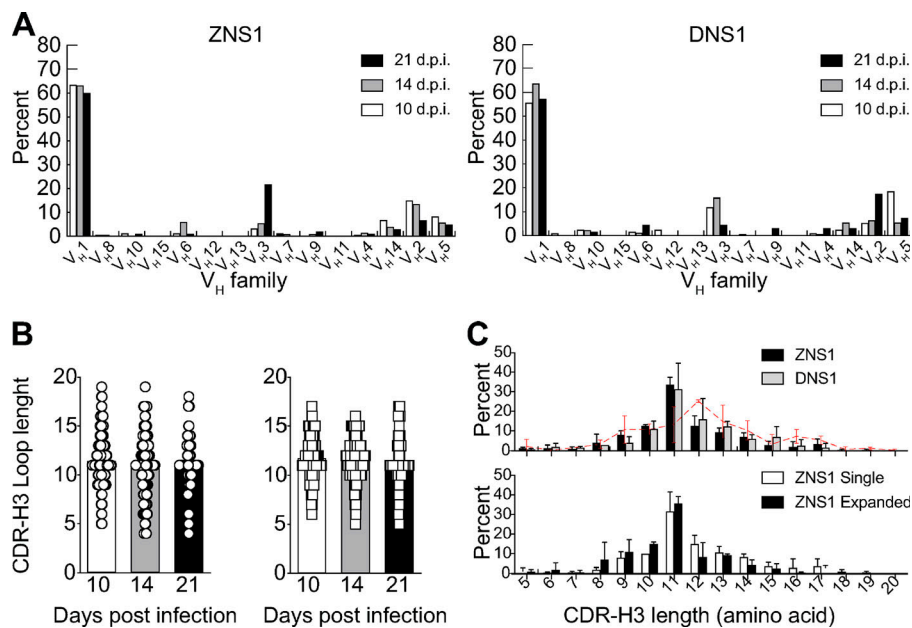


Figure S4. **Analysis of  $V_H$  family usage and CDR-H3 length of *Igh* transcripts from B cells present in GCs after ZIKV NS1 or DENV NS1 immunization.** **(A)** Expression of each  $V_H$  family as a percentage of total functional transcripts from GC B cells at each time point after immunization with ZIKV NS1 or DENV NS1. **(B)** CDR-H3 loop length variation at each time point after immunization with ZIKV NS1 or DENV NS1. **(C)** CDR-H3 loop length distribution of all sequences at all time points (upper panel) and comparison between clonal (clonotypes found more than once in the same LN) and single clones from mice immunized with ZIKV NS1 (lower panel). Dashed red line indicates the distribution of CDR-H3 length in FO B cells from WT BALB/c mice. GC B cells were sorted and sequenced from individual LNs and pooled for analyses (two to four mice per group from two independent experiments). Error bars represent SEM.

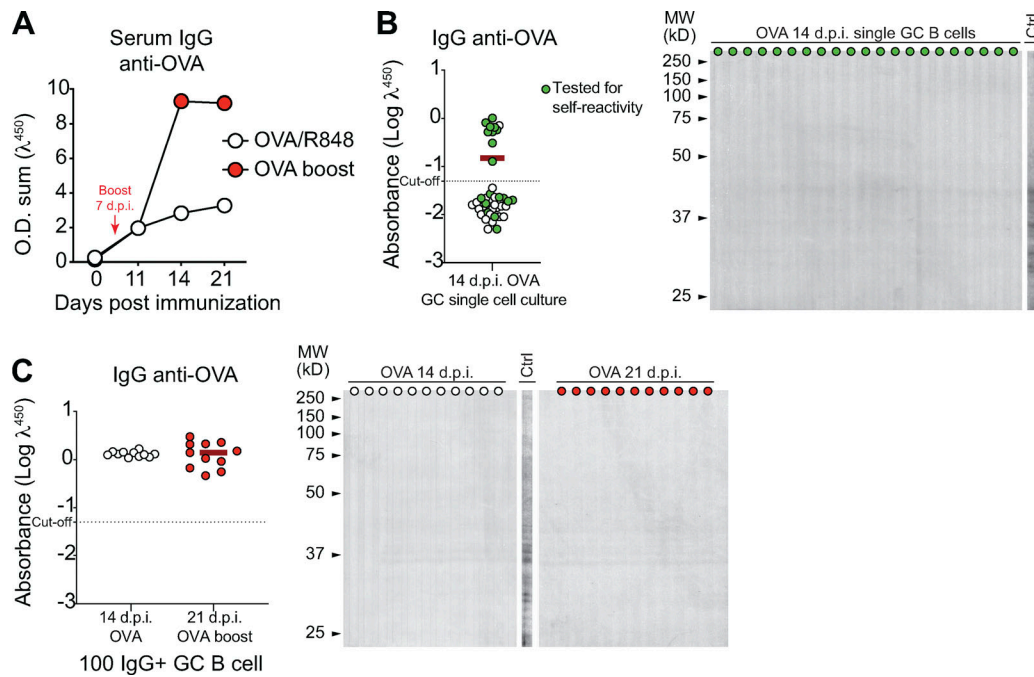


Figure S5. **Antigen specificity of B cells in GCs after immunization with OVA.** BALB/c mice were immunized s.c. with OVA (2  $\mu\text{g}/\text{mouse}$ ) combined with R848 (1  $\mu\text{g}/\text{mouse}$ ). When indicated, a booster immunization was performed on day 7 after prime. **(A)** Kinetics of serum levels of IgG binding to OVA, measured by ELISA. O.D. sum is the summation of ODs of four serum dilutions (1:40, 1:120, 1:360, and 1:1,080). **(B and C)** Single GC B cell (B) or pooled GC B cells (C) were sorted and cultured on a monolayer of gamma-irradiated NB21 feeder cells ( $10^3$  cells/well; Kuraoka et al., 2016). After 7 d, supernatants were collected for binding assays. Supernatants were screened for IgG production and IgG<sup>+</sup> wells were tested for binding to OVA protein by ELISA or immunoblot against mouse brain tissue as source of self-antigens. Ctrl, serum from ZIKV infected mice. One experiment was performed with three mice.

Tables S1 and S2 are provided online as separate Excel files. Table S1 lists CDR-H3 characteristics from GC B cell clones tested for self-reactivity. Table 2 lists *Igh* sequences and is related to Figs. 5 and 6.